RELATIVISTIC COULOMB EXCITATION OF THE PYGMY DIPOLE AND GIANT RESONANCES

A Thesis

by

Nathan S. Brady

Submitted to the Office of Graduate Studies
of Texas A&M University-Commerce
In partial fulfillment of the requirements
for the degree of
MASTER OF SCIENCE
December 2016

RELATIVISTIC COULOMB EXCITATION OF THE PYGMY DIPOLE AND GIANT RESONANCES

A Thesis

by

Nathan S. Brady

Approved by:

Advisor:	Carlos Bertulani
Committee:	Bao-An Li
	William Newton
Head of Department:	Matt Wood
Dean of the College:	Brent Donham
Dean of Graduate Studies:	Arlene Horne

Copyright © 2016

Nathan S. Brady

ABSTRACT

RELATIVISTIC COULOMB EXCITATION OF
THE PYGMY DIPOLE AND GIANT RESONANCES

Nathan S. Brady, MS
Texas A&M University-Commerce, 2016

Advisor: Carlos Bertulani, PhD

Nuclear collisions involving heavy charged nuclei traveling at relativistic speeds can bring one or both nuclei to an excited state. In collisions where the target is excited by the electromagnetic field of the projectile the process is called Relativistic Coulomb Excitation (RCE). Classical approximations are a good starting point for describing RCE, however, more accurate predictions require a quantum mechanical treatment.

Collisions which result in RCE have a certain probability to displace a large fraction of the nuclear matter inside a nucleus. This characteristic response is intrinsic to all nuclei containing more than a few protons and neutrons and is called a Giant Resonance (GR). Many classical and microscopic models have been used to describe this phenomenon including zero range Skyrme forces, Mean-field Approximations, and the Random Phase Approximation (RPA). As the number of neutrons become much larger than the number of protons within the nucleus the excess neutrons begin to form a skin beyond the typical charge radius. This neutron skin can be excited through RCE and cause the skin to oscillate against the strongly bound symmetric core. The strongest oscillation between the core and neutron skin is called the dipole mode and the resulting phenomenon is referred to as the Pygmy Dipole Resonance (PDR).

This thesis will look at how the PDR is influenced by the larger strength of the GR for interactions above 100 MeV/nucleon. As the dynamics of the collision changes, the probability of exciting a PDR changes considerably. The effects due to the coupling of the PDR to the GR indicates a need for improved theoretical studies for reactions at these collision energies.

ACKNOWLEDGMENTS

I would first like to thank my thesis advisor, Dr. Carlos Bertulani of the Physics Department at Texas A& M University-Commerce (TAMU-C). He was an exemplary mentor and I consider him to be a true friend. His guidance helped me through the most trying time of my career. I would also like to recognize Prof. Dr. Thomas Aumann of the Physics Department at Technische Universitat Darmstadt. Without his collaboration, the work presented here would not have been possible.

My future career has been enriched and made possible with the encouragement and support of both Dr. Matt Wood, head of the TAMU-C Physics Department and Dr. Bao-An Li, Regents professor of TAMU-C. The classes taught by each of them continue to be an invaluable resource as I move forward with my studies.

The friends I have made since joining the physics department at TAMU-C have been one of the most rewarding aspects of my life. In light of that, I would also like to acknowledge my fellow colleague, office-mate, and friend, James Thomas, who also worked under Dr. Bertulani. Lastly, I would like to acknowledge my family for their unwavering support and encouragement as I pursue my passion for physics. I must also thank Sarah Cantu for putting up with me through it all. Her support has been a major factor as I worked towards finishing this thesis.

Thank you,

- Nathan S. Brady

Contents

List of Figures

Chapter 1

INTRODUCTION

Understanding the principles by which our universe is guided and the laws that restrict its evolution have always been a large motivation for scientific discovery. Nuclear physics is the study of phenomena which govern the interactions between matter at the femtometer scale. These interactions are built up from the residue of the strong nuclear force, described by quantum chromodynamics, and are subject to electromagnetic interactions described through quantum electrodynamics.

Particle collisions are used to investigate the dynamics of interacting particles. Measurements are made by extracting information, (e.g., mass, momentum, spin, ...) carried by the products of these collisions and inferring the original conditions which produced the observations. The probability of producing a particular event is calculated through its cross section which tells us where to expect certain products produced by said event.

Statement of the Problem

In peripheral collisions the distance between the two nuclei under consideration are just large enough so as not to directly interact by the strong nuclear force. The event is then dominated by Coulomb interactions, and at relativistic speeds it is better known as Relativistic Coulomb Excitation (RCE), which is a well-established tool used for studies in nuclear structure [1]. During an RCE event, the electric field generated by the incident heavy-ion transfers energy to the nucleons within the other nucleus exciting it to a higher energy level. At certain excitation energies the nuclear response will be amplified considerably and is described as the characteristic resonance of the nucleus.

These characteristic resonances which dominate the low energy excitations around 8 MeV and higher for all nuclei with more than a few nucleons (i.e., protons and neutrons) are known as Giant Resonances (GR). These phenomena, first observed by Bothe and Gentner

in 1937 [2], were shown to have a high probability of photoabsorption at these energies. These phenomena are well studied, see for instance [3, 4] and theories, both classical and microscopic, reproduce the observations well. An associated phenomenon which appears in nuclei with more neutrons than protons is known as the Pygmy Dipole Resonance (PDR) and is the collective vibration of the neutrons against a symmetric nuclear core. Further reading on the pygmy resonance can be found in Ref. [5]

Purpose of the Study

The PDR was suggested in 1987 as a possible excitation in neutron-rich nuclei by Kubono, Nomura, and collaborators [7]. Theoretical support was later established by Ikeda [8] and collaborators. Experimental evidences for the existence of a collective low energy response in neutron-rich nuclei, far from the valley of stability, took nearly two decades more to emerge. Initially the direct breakup of light and loosely-bound projectiles, such as ^{11}Be and ^{11}Li were suggestive of a collective nuclear response, i.e., a PDR, but was later shown to be a direct Coulomb dissociation of the weakly-bound valence nucleons [9]. This suggests that the characteristics are poorly understood and further investigations, both experimentally and theoretically, are needed.

The intent of this study is to investigate the dynamics of these associated phenomena produced from RCE experiments. A coupling between the PDR and the various excited vibrational modes comprising the GR is investigated. The calculation of this coupling is important to investigate since the strength and energy of the PDR would be affected appreciably. This in turn would affect the calculation of the neutron skin, which is characterized by the PDR.

Hypothesis

The Coulomb excitation of PDR at 100 MeV/nucleon and above are investigated. As the dynamics of the collision evolve, the question of the influence on the PDR by the larger

GR is addressed.

- The coupling of the GR to the PDR will affect the excitation probability considerably.
- Different collision energies will affect the amount this coupling changes the cross section of the PDR.

Research Questions

An important aspect of investigating the PDR is the calculation of the neutron skin which tells us more about neutron matter and how it relates to neutron stars. We will attempt to answer the following questions:

- How does the collision energy affect the centroid energy and width of the PDR? How much does this change the calculation of the neutron skin and polarizability?
- How do the separate major modes of oscillation of the GR (i.e., Giant Dipole and Giant Quadrupole) affect the cross section of the PDR? Is there a preference to coupling with either of the modes?

Significance of the Study

A revitalized interest in neutron matter and nuclei far from the line of stability has emerged. The ability to measure the neutron radius has historically been an experimental challenge which stems from the neutral charge of the neutrons. Since the PDR has been shown to emerge in neutron-rich nuclei it has been suggested that it could be used to constrain the neutron skin thickness [6].

Accurate measurements of the neutron skin and extraction of the dipole polarizability are important for constraining the symmetry energy associated with the binding of nucleons in the nucleus. How the GR affects the PDR is then an important question; for small changes to the observed PDR the measurement of the neutron skin will be affected.

Method of Procedure

Since the objective was to determine how the multipole modes of the GR affected the PDR cross section, we utilized current predictions of both the PDR and GR's centroid energy and width. Two practical examples of reactions, ^{68}Ni + ^{208}Au and ^{68}Ni + ^{208}Pb, are used to facilitate discussions on the effect of coupling between the GR and the PDR.

Definition of Terms

Nucleon. The constituent particles of nuclei, i.e., protons and neutrons, which come together to form the nucleus of an atom. Elements differ by the number of protons, Z, and isotopes, elements with the same Z, differ by the number of neutrons, N. [3, 10]

Nuclei. Term which refers to the nucleus of all elements composed of nucleons. [3,10]

Differential Cross Section. Rate of scattered particles detected at some angle, $d\sigma/d\Omega$, where Ω is the solid angle. Interpreted as the probability of detecting a particle within the given solid angle. [3, 10]

Cross Section. An effective "area" which an interaction can occur. [3, 10]

Coulomb Interaction. Class of interactions between particles through their mutual electromagnetic fields. [11]

Nuclear Excitation. The observed reaction of nuclear matter to external stimuli resulting in the jump of one or more nucleons within the nucleus into a higher energy level. The nucleus is then said to be in an excited state. [3, 10]

Relativistic Coulomb Excitation. Excitation of a nucleus by the electromagnetic field of a charged particle moving at relativistic speeds. [12]

Multipole Expansion. The decomposition of the angular dependence of a potential into increasingly finer segments. Multipole moments comprising the first few terms of the expansion are defined as the Monopole ($l = 0$), Dipole ($l = 1$), and Quadrupole ($l = 2$) moments. [11]

Giant Resonance. A high-frequency collective nuclear response involving an appreciable number of nucleons. Characterized by the large photoabsorption cross section observed in all nuclei with more than a few nucleons. [3, 4]

Giant Dipole Resonance. The second and most prominent multipole moment of oscillation which makes up the Giant Resonance. Described as the collective vibration between the protons and neutrons. [3, 4]

Giant Quadrupole Resonance. The third multipole moment of oscillation and second largest contribution to the Giant Resonance. [3, 4]

Pygmy Dipole Resonance. Similar to a giant resonance, but with a smaller strength. [3, 4]

Limitations

Calculations utilize well known empirical data when necessary such as; the width of the resonance, location of the centroid energy, and total nuclear cross sections σ_{NN} corrected for in-medium interactions. The location of the Pygmy Dipole Resonance is taken from experimental data while the width used is more consistent with theoretical calculations. This restricts our analysis of results to be in a qualitative manner.

Delimitations

The low-energy resonances considered in this thesis are induced through the method of Relativistic Coulomb Excitation. Therefore, only heavy-ion reactions at 100 MeV/nucleon and above are considered. Since we are considering only Relativistic Coulomb Excitations,

we restrict ourselves to collisions at large impact parameters, i.e., no overlap of the two nuclei, so $b > R_1 + R_2$.

Organization of Thesis Chapters

Chapter 1 gives an outline of the study and motivations for this investigation. The problem of inducing the PDR and GR through Coulomb excitation is introduced, then a brief explanation of the coupling between the PDR and GR is given as the main focus of the thesis. Chapter 2 develops the theoretical background leading to the idea of relativistic Coulomb excitation in the context of nuclear reactions. We also show how the equivalent photon method can be used in the theory of relativistic Coulomb excitation and show how the idea of equivalent photons appears in many aspects of physics. The coupled-channels calculation, important for determining how the PDR and GR are coupled, is also introduced at the end of Chapter 2. Chapter 3 takes the ideas developed in the previous chapter and applies it to the development of nuclear physics. The giant and pygmy dipole resonances are introduced and theoretical models are briefly covered. Chapter 4 gives results on how the PDR is coupled to the GR. These results are then compared to current theoretical predictions using perturbation theory. Chapter 5 summarizes the results of the calculation and we give our conclusions.

Chapter 2

COULOMB EXCITATION

2.1 Underlying Theory

The theory of electrodynamics, which describes the interactions between charged particles, plays a pivotal role in modern physics and the development of the standard model. Forgoing the highly interesting yet impertinent pre-19^{th} century studies in electrostatics, I instead choose to begin with the monumental work of Maxwell in 1873 [13, 14], which stem from numerous experimental works including the equally notable, experimental physicist, Michael Faraday.

The second volume of Maxwell's treaties [14], brought together, in a mathematically coherent way, the presupposed distinct interactions of electricity and magnetism into a unified theory of electromagnetism with light as its propagator. In Maxwell's work a collection of differential equations describing the propagation of the electromagnetic fields through vacuum were formulated. These equations as amended by Heaviside are,

$$\nabla\cdot\mathbf{E} = \frac{\rho}{\epsilon_0} \tag{2.1}$$

$$\nabla\cdot\mathbf{B} = 0 \tag{2.2}$$

$$\nabla\times\mathbf{E} = -\frac{\partial\mathbf{B}}{\partial t} \tag{2.3}$$

$$\nabla\times\mathbf{B} = \mu_0\mathbf{J} + \mu_0\epsilon_0\frac{\partial\mathbf{E}}{\partial t} \tag{2.4}$$

setting $\rho = \mathbf{J} = 0$ for a charge free region, the vacuum equations are reproduced. In the case of electromagnetic fields in vacuum we may take the curl of both (2.3) and (2.4) and use the identity, $\nabla \times (\nabla \times \Phi) = \nabla(\nabla \cdot \Phi) - \nabla^2\Phi$, which gives the well known wave equation for electromagnetic radiation.

$$\frac{\partial^2 \mathbf{E}}{\partial t^2} = c^2 \cdot \nabla^2 \mathbf{E}$$
$$\frac{\partial^2 \mathbf{B}}{\partial t^2} = c^2 \cdot \nabla^2 \mathbf{B}$$

with the velocity of the wave, through a non-conducting medium, denoted by $c = (\epsilon_0 \mu_0)^{-\frac{1}{2}}$, the speed of light.

Maxwell's work did away with action at a distance and cemented the idea of fields into modern-day physics. The theory of electromagnetism has since been extended beyond its classical origins into a fully consistent quantum mechanical theory.

2.1.1 Potential Fields and Gauge Transformations

The Maxwell equations (2.1-2.4) are one of the greatest strides made in physics paving the way for more modern theories. Using vector notation as above it is immediately apparent that equation (2.2) has a freedom in defining the magnetic field as $\mathbf{B} = \nabla \times \mathbf{A}$ where the transformation $\mathbf{A} \rightarrow \mathbf{A} + \nabla\psi$ is made with $\psi(\mathbf{r}, t)$ arbitrary. Since the curl of any scalar vanishes, $\mathbf{B} = \nabla \times (\mathbf{A} + \nabla\psi) = \nabla \times \mathbf{A} + \cancelto{0}{\nabla \times \nabla\psi}$, the magnetic field remains unchanged.

Applying the transformation preserves the magnetic field, however, the electric field changes according to equation (2.3),

$$\begin{aligned}
\nabla \times \mathbf{E} = -\frac{\partial \mathbf{B}}{\partial t} \qquad \text{where} \quad \mathbf{B} &= \nabla \times \mathbf{A} \\
\Rightarrow \nabla \times \mathbf{E} &= -\frac{\partial}{\partial t}(\nabla \times \mathbf{A}) \\
&= \nabla \times \left(-\frac{\partial \mathbf{A}}{\partial t}\right) \\
\Rightarrow \quad \nabla \times &\left(\mathbf{E} + \frac{\partial \mathbf{A}}{\partial t}\right) = 0
\end{aligned}$$

Since the curl of a gradient is always zero we can assign the term inside the parenthesis equal

to the negative of some scalar potential ϕ so that,

$$\Rightarrow \quad \mathbf{E} + \frac{\partial \mathbf{A}}{\partial t} = -\nabla\phi$$

$$\therefore \qquad \mathbf{E} = -\nabla\phi - \frac{\partial \mathbf{A}}{\partial t} \tag{2.5}$$

Defining the magnetic field as the curl of some vector field $\mathbf{A}$ results in a new definition for the electric field given by equation (2.5). This is true for any arbitrary gauge. Now using the same transformation on equation (2.5),

$$\begin{aligned} \mathbf{E} = -\nabla\phi - \frac{\partial \mathbf{A}}{\partial t} \qquad & \text{where} \quad \mathbf{A} \to \mathbf{A} + \nabla\psi \\ \Rightarrow \qquad \mathbf{E} &= -\nabla\phi - \frac{\partial}{\partial t}\left(\mathbf{A} + \nabla\psi\right) \\ &= -\nabla\phi - \frac{\partial \mathbf{A}}{\partial t} - \nabla\frac{\partial \psi}{\partial t} \\ &= -\nabla\left(\phi + \frac{\partial \psi}{\partial t}\right) - \frac{\partial \mathbf{A}}{\partial t} \end{aligned}$$

by making a new transformation $\phi \to \phi - \dfrac{\partial \psi}{\partial t}$ equation (2.5) remains unchanged. This gives the final solutions to the partial differential equations (2.1 - 2.4) as,

$$\mathbf{E} = -\nabla\phi - \frac{\partial \mathbf{A}}{\partial t} \tag{2.6}$$

$$\mathbf{B} = \nabla \times \mathbf{A} \tag{2.7}$$

where $\mathbf{A}$ and ϕ are the magnetic vector and electric scalar potential fields respectively and are a consequence of the gauge freedom inherent of Maxwell's equations.

2.1.2 Lorenz Gauge

Many different gauges have been developed to exploit this "freedom" and is known as gauge fixing [11]. One such gauge transformation, which fits nicely with special relativity, is the Lorenz gauge. Named for the Danish physicist Ludvig Lorenz, it introduces a transformation to the scalar ϕ and vector $\mathbf{A}$ potentials while maintaining the solutions to the Maxwell equations (2.1 - 2.4) as above.

Beginning from equations (2.1) and (2.4) then inserting solutions (2.6) and (2.7), we get the equations of motion for a

$$\begin{aligned}
\nabla \cdot \mathbf{E} = \frac{\rho}{\epsilon_0} \quad \text{where} \quad \mathbf{E} &= -\nabla\phi - \frac{\partial \mathbf{A}}{\partial t} \\
\Rightarrow \quad \nabla \cdot \left(-\nabla\phi - \frac{\partial \mathbf{A}}{\partial t} \right) &= \frac{\rho}{\epsilon_0} \\
\therefore \qquad \nabla^2\phi + \frac{\partial \left(\nabla \cdot \mathbf{A} \right)}{\partial t} &= -\frac{\rho}{\epsilon_0} \qquad (2.8) \\
\nabla \times \mathbf{B} = \mu_0 \mathbf{J} + \mu_0 \epsilon_0 \frac{\partial \mathbf{E}}{\partial t} \quad \text{where} \quad \mathbf{B} &= \nabla \times \mathbf{A} \\
\Rightarrow \quad \nabla \times (\nabla \times \mathbf{A}) &= \mu_0 \mathbf{J} + \frac{1}{c^2} \frac{\partial}{\partial t} \left(-\nabla\phi - \frac{\partial \mathbf{A}}{\partial t} \right) \\
\Rightarrow \quad \nabla \left(\nabla \cdot \mathbf{A} \right) - \nabla^2 \mathbf{A} &= \mu_0 \mathbf{J} - \frac{1}{c^2} \frac{\partial}{\partial t} \nabla\phi - \frac{1}{c^2} \left(\frac{\partial^2 \mathbf{A}}{\partial t^2} \right) \\
\therefore \qquad \nabla^2 \mathbf{A} - \frac{1}{c^2} \left(\frac{\partial^2 \mathbf{A}}{\partial t^2} \right) &= -\mu_0 \mathbf{J} + \nabla \left(\nabla \cdot \mathbf{A} + \frac{1}{c^2} \frac{\partial \phi}{\partial t} \right) \qquad (2.9)
\end{aligned}$$

In equation (2.9) a necessary condition in order to preserve Maxwell's equations is,

$$\nabla \cdot \mathbf{A} + \frac{1}{c^2} \frac{\partial \phi}{\partial t} = 0 \qquad (2.10)$$

This is known as the Lorenz condition and allows us to write the equations of motion in

their final form,

$$\nabla^2\phi - \frac{1}{c^2}\frac{\partial^2\phi}{\partial t^2} = -\frac{\rho}{\epsilon_0} \tag{2.11}$$

$$\nabla^2\mathbf{A} - \frac{1}{c^2}\frac{\partial^2\mathbf{A}}{\partial t^2} = -\mu_0\mathbf{J} \tag{2.12}$$

where we used equation (2.10) to solve for $\nabla \cdot \mathbf{A}$ and insert into equation (2.8). These are the symmetric equations of motion for a charged particle.

By inspection we see a similarity between these and the wave equations for electromagnetic radiation in vacuum (i.e. $\rho = \mathbf{J} = 0$). Applying the transforms $\mathbf{A} \to \mathbf{A}_0 + \nabla\psi$ and $\phi \to \phi_0 - \partial\psi/\partial t$ to the Lorenz condition, equation (2.10) leads to,

$$\nabla \cdot \mathbf{A} + \frac{1}{c^2}\frac{\partial\phi}{\partial t} \quad \to \quad \nabla \cdot \mathbf{A}_0 + \frac{1}{c^2}\frac{\partial\phi_0}{\partial t} + \nabla^2\psi - \frac{1}{c^2}\frac{\partial^2\psi}{\partial t^2} = 0$$

where $\mathbf{A}_0$ and ϕ_0 are the original potentials. To preserve our original condition in equation (2.10) for our initial potentials $\mathbf{A}_0$ and ϕ_0 we require,

$$\nabla^2\psi - \frac{1}{c^2}\frac{\partial^2\psi}{\partial t^2} = 0$$

which is simply the wave equation for a scalar function $\psi(\mathbf{r}, t)$. This means that under the Lorentz gauge we have an infinite number of solutions which satisfy the Maxwell equations and everything is treated as a wave. This blends nicely with the implications of special relativity and naturally works in quantum mechanics where everything is a wave.

A Quantum Theory

The laws which govern our universe are quantum mechanical and any theory which hopes to succeed in its attempt to describe physical reality must be consistent with quantum

mechanics. The theory of quantum electrodynamics (QED) is marked as the first successful quantum field theory, consistent with relativity. Due to the tremendous success of QED, it has become the standard measure of a theory's acceptance.

In our formulation of QED the interaction between charged particles (e.g., electrons, protons, mesons, ...) is through the exchange of photons. These photons are the mediators of the electromagnetic force. The use of Feynman diagrams, introduced by Richard Feynman in the 1940s, has become the preferred method in describing particle interactions.

This pictorial method was a simple way of tracking the overwhelmingly diverse interactions plaguing QED at the time. Following Feynman's steps provided a systematic approach in diagramming these interactions.

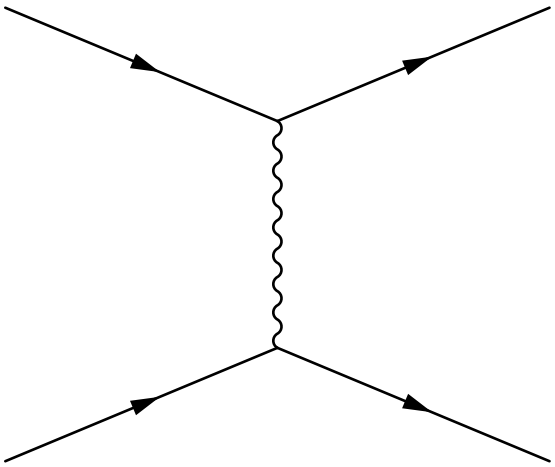

Figure 2.1. Interactions between fermions can be represented by a Feynman diagram. The solid lines represent fermions and the wavy line is the force carrier, i.e., the virtual photon.

Figure 2.1 gives the standard depiction of electron scattering, depicted as a Feynman diagram. In 2.1 the horizontal axis represents the forward flow of time while the vertical axis gives motion in 3-space. Fermions are represented by solid lines while the virtual photon (wavy line) is the mediator of the electromagnetic interaction. This virtual photon connecting the two particles removes the need for action at a distance. For a more in depth discussion on QED and the use of Feynman diagrams in quantum field theory refer to Peskin and Schroeder [15].

The development of this beautiful concept of gauge boson exchange as the force car-

riers revolutionized theoretical nuclear/particle physics, beginning with the photon as the mediator for the Coulomb interaction. Using this concept we proceed into discussions of nuclear interactions, a many-body quantum problem. Starting with, as one might expect, a classical approximation to the process of Coulomb excitation.

2.2 Nuclear Excitation

Excitation of nuclei by means of providing energy through electromagnetic interactions is known as Coulomb excitation. This situation is observed most easily in nuclear collisions where a target nucleus is perturbed by an external electromagnetic field. This may be achieved through a number of ways, however, the excitation through scattering particles will be this works focus.

2.2.1 Heavy-Ion Collisions

When the number of protons and neutrons involved in a nuclear collision becomes large we refer to these as heavy ion collisions. These heavy nuclear collisions present a dynamic system with a very rich collection of interesting phenomenon.

In this situation a charged ion Z_1 interacts with another charged particle Z_2 through the exchange of a photon

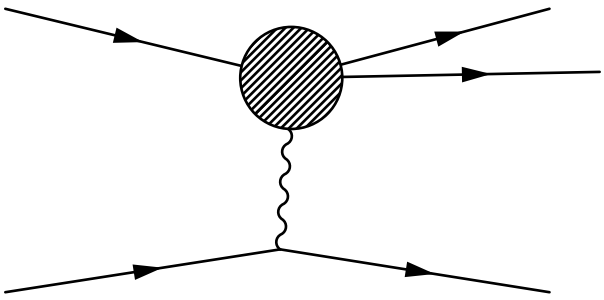

Figure 2.2. The interaction picture for a particle (lower solid line) colliding with a nuclear target (shaded circle), through the exchange of a virtual photon. The products are depicted by the outgoing solid lines.

Figure 2.2 gives a diagram representation of two interacting nuclei Z_1 and Z_2 where

the charged particles are shown to interact through the Coulomb force, represented by a mediating particle the photon (wavy line). This idea of photon exchange will be central to our discussions later. The three outgoing particles are what results from the interaction and are the only things observed. By looking at the incoming particles and measuring the outgoing products the scientist can reconstruct what interaction took place.

Several different ways to represent these types of interactions exist. However, the simplest method is to use Feynman diagrams. The benefit of including, implicitly, the conservation laws through vertex analysis still makes it preferable to other methods. For a brief overview of Feynman diagrams and rules see [15, 16].

2.2.2 Classical Scattering

Early investigations into nuclear physics typically involved low energy interactions between charged particles of low mass, e.g., electrons, protons, alpha particles, and a fixed target nucleus. The most notable of these experiments, which revealed the nucleus as being composed of a dense central core surrounded by electrons, were conducted by Ernest Rutherford.

In the aforementioned series of experiments, often called the Rutherford gold foil experiments, the low energy scattering of an alpha particle beam off a target of thin gold foil resulted in the detection of scattered alpha particles back towards the source. Backscattering as it's now called can be represented as a one-body elastic scattering problem which describes the trajectory of an incident charged particle as it interacts with a central force.

Scattering particles is still the preferred method used to investigate nuclear structure. Since the need to probe deeper into the nucleus is more necessary, scattering particles achieves this by increasing the interaction energy and decreasing the impact parameter of the colliding nuclei. This requires the construction of larger and more powerful colliders.

Rutherford

Rutherford scattering, as the low energy method is more commonly referred, is the classical approximation to a quantum mechanical system. In this system the interacting particles carry with them a charge, $Z_{(1,2)}e$, and momentum, $p_{(1,2)}$, where the indices denote projectile and target, respectively. A particle is said to be scattered when its direction

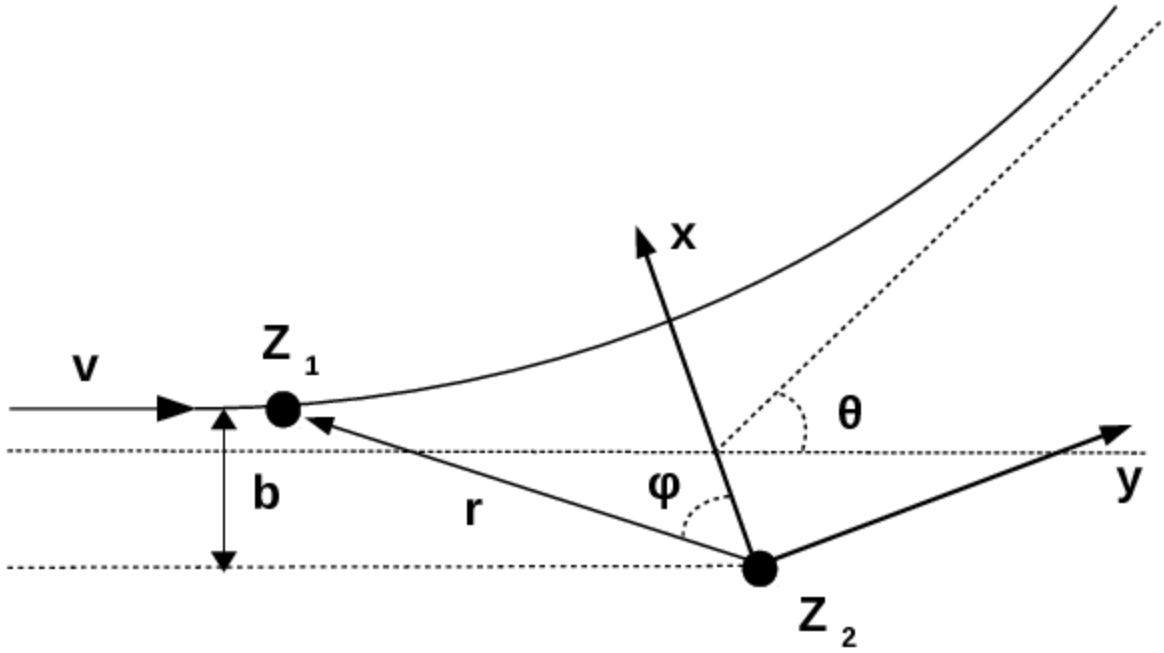

Figure 2.3. Scattering of an incident beam of particles by a center of force.

of motion is altered. Coulomb proved that the electric force follows an inverse-square law similar to the gravitational force which implies that the orbital equations are applicable, in the classical limit.

Given the charge of each particle and their relative velocity, v at infinity, we may calculate the strength of the Coulomb interaction by the Sommerfeld parameter

$$\eta = \frac{Z_1 Z_2 e^2}{\hbar v}. \tag{2.13}$$

A classical approximation is appropriate when, $\eta \gg 1$. This is possible when either, $Z_1 Z_2 \gg$

137, or, $v \ll c$. The trajectory of the projectile, Z_1, approaches the target, Z_2, as in Figure 2.3. The collisions considered in classical scattering are not strong enough to overcome the Coulomb barrier. However, we must consider the distance of closest approach, a, between the two nuclei. From the conservation of energy,

$$E = \frac{1}{2} m v_0^2 = \frac{Z_1 Z_2 e^2}{a}$$

we solve for a giving the distance in terms of the charges and relative speed,

$$a = \frac{2 Z_1 Z_2 e^2}{m v_0^2}$$

This is an important parameter since it gives us a known value in the projectile's trajectory.

In this arbitrary collision the trajectory of the projectile is dependent on the impact parameter and its kinetic energy. The "scattering angle", Θ, is uniquely determined for classical scattering. A scattered particle, in relation to the target, is observed passing through a cross sectional area $\sigma(\mathbf{\Omega})$. The area scattered is dependent on the scattering angle $\mathbf{\Omega}$. For a small segment of the scattering angle $d\Theta$ multiplied over the azimuthal coordinate $2\pi \sin\Theta$ the portion of solid angle is written as $d\Omega = 2\pi \sin\Theta \; d\Theta$.

Scattering strength is determined by the energy and angular momentum l. The angular momentum of a particle or planet is given as,

$$l = b\, p_0 = b\sqrt{2mE}$$

where $p_0 = m v_0$ is momentum and b is called the "impact parameter". The impact parameter is the distance between the centers of two scattering particles. Assuming from a classical perspective that particles at different impact parameters will have different scattering angles, the number of particles scattered are determined by the beam intensity, $I = N/A$, where N is the total number of incident particles passing through area A.

Using the differential cross section $\sigma(\mathbf{\Omega})$ defined as the flux, $\Phi(\mathbf{\Omega})$ of particles per beam intensity we have,

$$\sigma(\mathbf{\Omega}) = \frac{\Phi(\mathbf{\Omega})}{I} \tag{2.14}$$

We can solve for the number of particles scattered into solid angle $d\Omega$ by using the definition of flux, $\Phi(\mathbf{\Omega}) = dn/d\Omega$. The number of particles, n, incident on the target is dependent on the impact parameter as well as the scattering angle allowing the flux to be written as,

$$\Phi(\mathbf{\Omega}) = \frac{dn}{dA} \cdot \frac{dA}{d\Omega}$$

where $I = dn/dA$, the incident beam intensity. Inserting into equation (2.14) we have,

$$\sigma(\mathbf{\Omega}) = \frac{\Phi(\mathbf{\Omega})}{I}$$

$$\Rightarrow \qquad I\,\sigma(\mathbf{\Omega}) = \frac{dn}{dA} \cdot \frac{dA}{d\Omega}$$

multiplying by $d\Omega$ on both sides and substituting in $I = dn/dA$ we get,

$$I\,\sigma(\mathbf{\Omega})\,d\Omega = I\,dA$$

$$\Rightarrow \qquad 2\pi I\,\sigma(\Theta)\sin\Theta\,d\Theta = 2\pi I\,b\,db$$

where we used the incident beam cross section $A = \pi b^2 \quad \Rightarrow \quad dA = 2\pi b\,db$. The differential cross section is now dependent on the scattering angle Θ, solving for $\sigma(\Theta)$ gives,

$$\sigma(\Theta) = \frac{b}{\sin\Theta}\left|\frac{db}{d\Theta}\right| \tag{2.15}$$

a straightforward relation between the impact parameter and the scattering angle measured. Additionally deriving the impact parameter from the eccentricity of a hyperbolic orbit equa-

tion (2.15) becomes,

$$\sigma(\Theta) = \frac{1}{4}\left(\frac{ZZ'e^2}{2E}\right)^2 \csc^4\frac{\Theta}{2} \tag{2.16}$$

the famous Rutherford Scattering equation. The relationship between equations (2.15) and (2.16) can be found in Goldstein's *Classical Mechanics*. [17] Rutherford's equation is relevant for low energy scattering where the incoming particle doesn't penetrate the targets Coulomb barrier such as the gold foil alpha particle scattering. Once the projectile and target begin to overlap, e.g., 25 MeV for α+Pb, the scattering becomes inelastic and Rutherford's equation no longer applies.

2.3 Semi-classical Theory of Coulomb Scattering

The validity of a semi-classical approach to the method of Coulomb excitation is well-known for studies on nuclear excitation. As stated before it provides a way to study reactions without having to include the many-body nuclear forces. This is a well established method and has been extensively covered by several investigators.

In the electromagnetic excitation process we describe an interaction Hamiltonian as

$$\mathbf{H}_{int} = \mathbf{H}_P + \mathbf{H}_T + \mathbf{V}(\mathbf{r}(t))$$

where the matrix $\mathbf{H}_P(\mathbf{H}_T)$ is the projectile(target) Hamiltonian and $\mathbf{V}(t)$ is a time-dependent term describing the electromagnetic interaction between both projectile and target.

An appropriate choice for the frame of reference (i.e., target or projectile) reduces the above interaction Hamiltonian. In our treatment of the problem we choose the frame of reference of the target and consider only stable projectiles with the ground state Hamiltonian $\mathbf{H}_T$. The excitation is then built from the ground state of the target. The new Hamiltonian

must satisfy the time-dependent Schrödinger equation

$$\mathbf{H}_{int}\mathbf{\Psi}(t) = i\hbar\frac{d\mathbf{\Psi}(t)}{dt} \tag{2.17}$$

Performing an expansion on the total time-dependent wave function $\mathbf{\Psi}(t)$ in terms of the set of orthogonal eigenfunctions which form a complete basis

$$\mathbf{\Psi}(t) = \sum_n a_n(t)\boldsymbol{\psi}_n e^{-iE_nt/\hbar} \tag{2.18}$$

where the ground state Hamiltonian of the target nucleus satisfies the eigenvalue equation

$$\mathbf{H}_T\boldsymbol{\psi}_n = E_n\boldsymbol{\psi}_n \tag{2.19}$$

using the newly expanded wave function (2.18) with the interaction Hamiltonian given as

$$\mathbf{H}_{int} = \mathbf{H}_T + \mathbf{V}(t)$$

we obtain a new form of the time-dependent Schrödinger equation (2.17) given as

$$i\hbar\frac{d}{dt}\left(\sum_n a_n(t)\boldsymbol{\psi}_n e^{-iE_nt/\hbar}\right) = \big(\mathbf{H}_T + \mathbf{V}(t)\big)\sum_n a_n(t)\boldsymbol{\psi}_n e^{-iE_nt/\hbar}$$

$$i\hbar\sum_n\left(\dot{a}_n(t) - \frac{iE_n}{\hbar}a_n(t)\right)\boldsymbol{\psi}_n e^{-iE_nt/\hbar} = \sum_n a_n(t)\left(\mathbf{H}_T + \mathbf{V}(t)\right)\boldsymbol{\psi}_n e^{-iE_nt/\hbar}$$

Distributing through on both sides of the equation and using the relation (2.19) we are left with the equation,

$$i\hbar\sum_n \dot{a}_n(t)\boldsymbol{\psi}_n e^{-iE_nt/\hbar} = \sum_n a_n(t)\mathbf{V}(t)\boldsymbol{\psi}_n e^{-iE_nt/\hbar}$$

multiplying both sides by ψ_m^* and integrating over all space we have

$$i\hbar \sum_n \dot{a}_n(t) e^{-iE_n t/\hbar}\ \delta_{mn} = \sum_n a_n(t) \left(\int_{-\infty}^{\infty} d^3r\ \boldsymbol{\psi}_m^* \mathbf{V}(t) \boldsymbol{\psi}_n \right) e^{-iE_n t/\hbar}$$

$$i\hbar\ \dot{a}_m(t) e^{-iE_m t/\hbar} = \sum_n a_n(t) \mathbf{V}_{mn}(t) e^{-iE_n t/\hbar}$$

where we used $\int_{-\infty}^{\infty} d^3r\ \boldsymbol{\psi}_m^* \boldsymbol{\psi}_n = \delta_{mn}$. The matrix elements for the electromagnetic interaction potential are given as

$$\mathbf{V}_{mn} = \int_{-\infty}^{\infty} d^3r\ \boldsymbol{\psi}_m^* \mathbf{V}(t) \boldsymbol{\psi}_n = \langle m|V(t)|n\rangle$$

solving for the differential time dependent amplitude of state m gives,

$$\Rightarrow \qquad \dot{a}_m(t) = -\frac{i}{\hbar} \sum_n \langle m|V(t)|n\rangle\ a_n(t) e^{i(E_m - E_n)t/\hbar} \tag{2.20}$$

We now have a set of m coupled equation where the sum runs over all possible excitation states n. The solutions to which are typically found by performing a multipole expansion on the potential $\mathbf{V}(\mathbf{r}(t))$. The Multipole expansion is introduced in the next section.

Equation (2.20) can be interpreted as the transition amplitude of a particle from an initial state $|i\rangle$ to some final state $|f\rangle$ with excitation $\hbar\omega = E_f - E_i$. The excitation is taken as the Fourier component to the transition frequency of the interaction Hamiltonian so that we have,

$$a_{fi}(t) = -\frac{i}{\hbar} \int_{-\infty}^{\infty} \langle f|H_{int}|i\rangle\ e^{i(E_f - E_i)t/\hbar} dt \tag{2.21}$$

The term $\langle f|H_{int}|i\rangle$ is the matrix form of the interaction Hamiltonian.

Integrating over a short time interval the transition amplitude is then,

$$a_m(t) = -\frac{i}{\hbar} \int_0^T \mathbf{V}_{mn}(t) e^{i(E_m - E_n)t/\hbar} dt \tag{2.22}$$

since for short time intervals the system returns to its original state ψ_m so that $a_n(t) = 1$ for $m = n$ else $a_n(t) = 0$.

Multipole Expansion

A multipole expansion of a potential is a way to approximate the effective electromagnetic interaction between charged particles in terms of their intrinsic coordinates. In spherical polar coordinates this takes separate treatment of the radial, polar, and azimuthal coordinates, r, θ, and ϕ respectively.

The Coulomb potential measured at $\mathbf{r}$ for a system of point-like charged particles e_i located at $\mathbf{r}_i$ is given in general by the equation

$$V(\mathbf{r}) = \sum_i \frac{e_i}{|\mathbf{r} - \mathbf{r}_i|} \tag{2.23}$$

$$\frac{1}{|\mathbf{r} - \mathbf{r}'|} \equiv (r^2 + r'^2 - 2rr' \cos\gamma)^{-1/2} \tag{2.24}$$

where the primed coordinates indicate the location of charged particles and $\cos\gamma = \cos\theta\cos\theta' + \sin\theta\sin\theta'\cos(\phi - \phi')$ is the angle between the primed and unprimed vectors.

Equation (2.24) depends on only the lengths of vectors $\mathbf{r}$ and $\mathbf{r}'$ and the angle between them γ. This allows a multipole expansion to be made in terms of the mutually orthogonal Legendre polynomials of order l.

$$\frac{1}{|\mathbf{r} - \mathbf{r}'|} = \frac{1}{r_>} \sum_{l=0}^{\infty} \left(\frac{r_<}{r_>}\right)^l P_l(\cos\gamma)$$

where $r_<$ ($r_>$) is the lesser(greater) distance between r and r'. By the addition theorem, as given in Appendix B of [18], a generalization to the geometric relation given by $\cos\gamma$. This leads to an expression for the Legendre polynomial as a linear combination of spherical

harmonics, of order l,

$$P_l(\cos\gamma) = \frac{4\pi}{2l+1}\sum_{m=-l}^{l} Y^*_{lm}(\theta',\phi')Y_{lm}(\theta,\phi)$$

leading to a final form for the expansion given as,

$$\frac{1}{|\mathbf{r}-\mathbf{r}'|} = \frac{1}{r_>}\sum_{l=0}^{\infty}\frac{4\pi}{2l+1}\left(\frac{r_<}{r_>}\right)^l \sum_{m=-l}^{l} Y^*_{lm}(\theta',\phi')Y_{lm}(\theta,\phi)$$

Applying the above expansion, given in terms of spherical harmonics for each discrete point charge i at $\mathbf{r}'$, equation (2.23) becomes,

$$V(\mathbf{r}) = \sum_{lm}\frac{4\pi}{2l+1}\frac{1}{r^{l+1}}Y^*_{lm}(\theta,\phi)\mathcal{M}(El,m) \tag{2.25}$$

where $\mathcal{M}$, the *electric multipole moment*, is given as,

$$\mathcal{M}(El,m) = \sum_i e_i r_i^l\, Y_{lm}(\theta_i,\phi_i), \qquad m = -l,-l+1,\ldots,l-1,l$$

The sum is over each electric charge e_i with position $\mathbf{r}_i = (r_i,\theta_i,\phi_i)$. Modifying the equation above, using the density operator

$$\rho(\mathbf{r}) = \sum_i e_i\delta(\mathbf{r}-\mathbf{r}_i),$$

the multipole moment $\mathcal{M}(El,m)$ is now a tensor operator of rank l. Integrating over all space the operator takes on the general form,

$$\mathcal{M}(El,m) = \int d^3r\rho(\mathbf{r})r^l Y_{lm}(\mathbf{n}), \qquad \mathbf{n} = \frac{\mathbf{r}}{r} \tag{2.26}$$

One postulate of quantum mechanics states that, for any measurable system which

has an associated physical observable can be represented by an operator. The multipole expansion of equation (2.23) into (2.25) puts it into a special class of quantum mechanical operators called the spherical tensor operators.

2.4 Relativistic Coulomb Excitation

In the previous section we expanded the potential in terms of its multipoles and put the multipole moment in the form of an operator, a necessary step for its use in quantum mechanics. Now we must go further and put the method of Coulomb Excitation into terms that are consistent with relativity.

The premise of Relativistic Coulomb Excitation (RCE) is taken from its low energy origins. As with Coulomb Excitation the fundamental assumption of RCE is that the nuclei do not interpenetrate. Reactions of this nature due to this process are short lived and enhanced due to Lorentz contraction of the field.

For the case of a projectile with energy, $E_{lab} \geq 100$ MeV/nucleon, the trajectory is nearly straight, i.e., negligible deflection, giving an interaction distance equal to the impact parameter b. We also consider only interactions involving the electric field and the target or projectile, so that, $b > R_T + R_P$, is larger than the sum of the radii of the target and projectile, respectively.

Using the same setup as with Coulomb Excitation, where we are in a target centered frame with the z-axis being the path of the projectile, we consider the case where $v \simeq c$. A particle traveling at these high energies will be Lorentz contracted in the direction of motion and can be described by the Liénard-Wiechert potential,

$$\phi(\mathbf{r}, t) = \frac{\gamma Ze}{\sqrt{(x-b)^2 + y^2 + \gamma^2(z-vt)^2}},$$

where b is the impact parameter and the factor $\gamma = (1 - v^2/c^2)^{-1/2}$ is the Lorentz factor making the component of the electric field parallel to the direction of motion, $+z$, compact

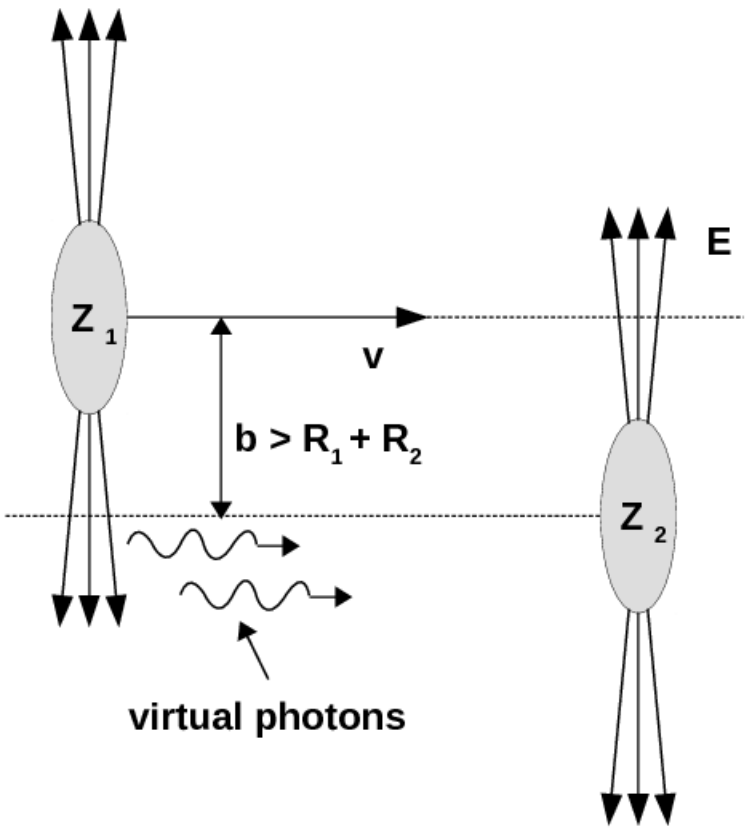

Figure 2.4. A relativistic charged projectile incident on a target with impact parameter larger than the strong interaction radius. The transfer of virtual photons is shown (wavy lines) coming from the Lorentz contracted i.e., pancake shaped, electromagnetic field.

and pancake like.

The above equation is the same electric potential field from our discussions on Lorenz gauge. The vector potential field used for a spinless particle following a classical trajectory is,

$$\mathbf{A}(\mathbf{r},t) = \frac{\mathbf{v}}{c}\,\phi(\mathbf{r},t)$$

where the velocity vector $\mathbf{v} = v\hat{\mathbf{z}}$. A multipole expansion can be made to the Liénard-Wiechert potential in a similar way as was done in the previous section.

Knowing the electric and vector potential field equations we can easily obtain the

associated electric and magnetic field equations from equations (2.6) and (2.7),

$$E_z = -\frac{Ze\gamma vt}{(b^2+\gamma^2v^2t^2)^{3/2}}$$

$$\mathbf{E}_T = \frac{Ze\gamma\mathbf{b}}{(b^2+\gamma^2v^2t^2)^{3/2}}$$

$$\mathbf{B}_T = \frac{\mathbf{v}}{c}\otimes\mathbf{E}_T, \qquad \text{and} \quad B_z = 0$$

where the equations are separated by components parallel(tangent) to the direction of motion and are denoted by subscript z(T).

For fast moving charged particles the interaction of the field on the target is short. That is for $\gamma \gg 1$, by inspection of the denominator, the time is approximately,

$$\gamma vt = b \qquad \rightarrow \quad t = \frac{b}{\gamma v} \simeq \frac{b}{\gamma c}$$

This shows the fields to be similar to two pulses of plane-polarized radiation. In the case for radiation along the z direction, this is an exact analogy. Radiation along the T direction is only approximate due to the presence of a magnetic field, however, this does not appreciably affect the dynamics of the system. At speeds $v = c$ the effects of the E_z field are minimal and allow us to add an additional field, $B = vE_z/c$. A calculation of the energy incident per unit area on the target due to an electromagnetic wave is now possible. Fourier transforming the Poynting vector $\mathbf{S} = \mathbf{E}\otimes\mathbf{B}$, the intensity of radiation, $I(\omega, b)$, is calculated with energy $E_\gamma = \hbar\omega$.

The probability of nuclear transition is then given by the integral,

$$P(b) = \int I(\omega,b)\sigma_\gamma(E_\gamma)dE_\gamma = \int n(\omega,b)\sigma_\gamma(E_\gamma)\frac{d\omega}{\omega} \tag{2.27}$$

where $\sigma(E_\gamma)$ is the photonuclear cross-section for photons of energy E_γ and $n(\omega, b)$ is the

number of equivalent photons in the electromagnetic wave at frequency ω and impact parameter b.

The term $n(\omega, b)$ in the above equation was first introduced by Enrico Fermi [19] who proposed that the electromagnetic field created by a charged particle can be equated to a flux of virtual photons. This idea of virtual photons mediating the electromagnetic interaction is obviously an important part to the theory of electromagnetism both classically (low energy scattering) and, as discussed above, quantum mechanically (QED).

Fermi's work, published in 1924 by Zeitschrift für Physik and also, unconventionally, published in Italian by Nuovo Cimento [20], was extended by Weizsäcer and Williams [21] to be used at relativistic velocities. This was essentially restoring the Lorentz factors in their proper places.

What remains to be shown is how this Lorentz contracted electromagnetic field interacts with a target possessing charge.

2.4.1 Equivalent Photon Method

The electromagnetic field of a fast moving charged particle is Lorentz contracted in the direction of motion. Considering only collisions where the nuclei do not overlap, i.e., impact parameter $b > R_P + R_T$, which is the case for Coulomb excitation, the probability can be expressed in terms of the sum over all transition probabilities into a final state I_f. The probability of Coulomb excitation is given as,

$$P_C(b, E_\gamma) = \sum_f \int P_{i\to f}(b)\rho_f(E_\gamma)dE_\gamma \tag{2.28}$$

where the sum is over all possible final states with the density of final states integrated over all energy transfers $E_\gamma = \hbar\omega = E_f - E_i$. The transition probabilities $P_{i\to f}$ are obtained from

the transition amplitude calculated in equation (2.21) so that,

$$P_{i\to f}(b) = \frac{a^2\epsilon^4}{4}\frac{1}{2I_i+1}\sum_{M_i,M_f}\left|a_{if}\right|^2$$

Using Wigner-Eckart theorem and respecting the orthogonality conditions of the Clebsh-Gordon coefficients, which produce delta functions from the expansion coefficients between angular momentum eigenstates, the transition probability can be expressed in the form,

$$P_{i\to f} = Z_1^2 e^2 \frac{4\pi^2 a^2 \epsilon^2}{\hbar^2}\sum_{\pi LM}\frac{B(\pi L, I_i\to I_f)}{(2L+1)^3}\left|S(\pi L, M)\right|^2 \tag{2.29}$$

again where $\pi =$ E or M and $B(\pi L, I_i \to I_f)$ is the reduced transition probability given as,

$$\begin{aligned} B(\pi L, I_i\to I_f) &= \frac{1}{2I_i+1}\sum_{M_i,M_f}\left|\langle I_i M_i|\mathcal{M}(\pi L, M)|I_f, M_f\rangle\right|^2 \\ &= \frac{1}{2I_i+1}\left|\langle I_i|\left|\mathcal{M}(\pi L)\right|\,|I_f\rangle\right|^2 \end{aligned}$$

The transition probability given by equation (2.29) can now be plugged into equation (2.28). If we use the idea proposed by Enrico Fermi to approximate the interaction of the electric field as a flux of virtual photons as in equation (2.27) then the probability becomes,

$$P_C(b, E_\gamma) = \sum_{\pi L} P_{\pi L}(b, E_\gamma) = \sum_{\pi L}\int \frac{dE_\gamma}{E_\gamma}\; n_{\pi L}(b, E_\gamma)\sigma_\gamma^{\pi L}(E_\gamma)$$

where the sum is now over multipole states. The term $n_{\pi L}(b, E_\gamma)$ is the virtual photon numbers and $\sigma_\gamma^{\pi L}$ is the photonuclear cross section for a given multipole.

2.4.2 Coupled-Channels

Coulomb Excitations are often dominated by transitions between the ground state and a continuum resonance state. Excitation into these states are treated as exact in a coupled-channels approach [22] where additional states are calculated as perturbations from

the ground state.

In the coupled-channels approach an excitation into a continuum of states is called a doorway state, or the particular entrance taken into the continuum. The ground state is then coupled to the set of doorway states creating a coupling matrix. Amplitudes for such excitations are given as,

$$\alpha^{(n)}(E_\gamma) = \langle \phi(E_\gamma) | \mathcal{D}^{(n)}_{LM} \rangle$$

and can be used as an expansion of the ground state potential. Integrating over all energy separations $\epsilon = E_\gamma - E_n$, where E_γ is the energy from the interaction and E_n is the centroid energy of the resonance n. Taking, for example, the dominant E_1 excitation and summing over all magnetic quantum numbers the time-dependent transition amplitude, equation (2.20), in the ground state is expressed as,

$$\begin{aligned}
\dot{a}_0(t) &= -\frac{i}{\hbar} \sum_M \int d\epsilon \langle \phi(\epsilon) | \mathcal{D}^{(1)}_{1M} \rangle \langle \mathcal{D}^{(1)}_{1M} | V_{E1,M}(t) | 0 \rangle \; a^{(1)}_{\epsilon,1M}(t) \exp\left\{ -i(E_1 + \epsilon)t/\hbar \right\} \\
&= -\frac{i}{\hbar} \sum_M \int d\epsilon \; \alpha^{(n)}(\epsilon) V^{(01)}_M(t) a^{(1)}_{\epsilon,1M}(t) \exp\left\{ -i(E_1 + \epsilon)t/\hbar \right\} \qquad (2.30)
\end{aligned}$$

where the dominant resonance amplitude is given as,

$$\frac{d}{dt} a^{(1)}_{\epsilon,1M}(t) = -\frac{i}{\hbar} \left[\alpha^{(1)}(\epsilon) \; V^{(01)}_M(t) \right]^* \exp\left\{ i(E_1 + \epsilon)t/\hbar \right\} \qquad (2.31)$$

Integrating (2.31) over time and using the result in equation (2.30) the result is,

$$\begin{aligned}
\frac{da_0}{dt}(t) = -\frac{1}{\hbar^2} \sum_M V^{(01)}_M(t) \int d\epsilon \left| \alpha^{(1)}(\epsilon) \right|^2 \\
\times \int_{-\infty}^{t} dt' \left[V^{(01)}_M(t') \right]^* \exp\left\{ -\frac{i}{\hbar}(E_1 + \epsilon)(t - t') \right\} a_0(t')
\end{aligned}$$

where $a^{(1)}_{\epsilon,1M}(t = -\infty) = 0$ was used and the squared amplitude term $\left| \alpha^{(1)}(\epsilon) \right|^2$ is chosen depending on the shape of the resonance.

Chapter 3

NUCLEAR STRUCTURE

Nuclear physics is one of the largest areas of research and continues to be a significant area of interest. Since its conception it has contributed to many fields including the field of astrophysics, problems in energy generation, medical technology, archaeological carbon dating, and even spawned the field of particle physics.

Early nuclear studies focused on the characterization of elements according to their constituent particles i.e., protons, electrons, and later neutrons. With the discovery of the neutron we had the final piece to a description of the nucleus, consistent with Einstein's mass-energy relation. With the neutrons discovery the energy contribution to the binding of a nucleus was finally calculable.

A new look at the elements, tabulated according to the ratios of protons to neutrons, was developed. From this point of view the binding energy, which apportions energy contributed by the constituents of the nucleus expended to the confinement of the nucleons due to the binding energy. The remaining energy constitutes the measured mass of the element.

The advent of this refined measurement to nuclear mass lead to questions apropos of the mechanism behind the confinement of neutrons and more interestingly the protons. Remembering the important relation from electrostatics, like charges repel, the protons within a nucleus, being in close proximity to one another, must feel concurrently opposing forces. These concurrent forces imposed on individual protons within the nucleus must be overcome by a much larger attractive force for a nucleus to form. This "strong force", which opposes the repulsive force of the protons, binds nucleons together and is contained within the description of the binding energy. However, its effective range of influence must be shorter than the electromagnetic interaction since it is not observed outside the nucleus.

Hideki Yukawa, in 1935 proposed a ground breaking theory to explain the binding of nucleons by the strong force [23]. Yukawa's model of the strong force was analogous to

the mediating photon model of the electromagnetic force where a low mass virtual particle is exchanged between the nucleons effectively binding them together. A straightforward calculation can be made to estimate this exchange. Using Heisenberg's uncertainty relation,

$$\Delta E \Delta t > \hbar$$

which states that the uncertainty in time and energy must be greater than Planck's constant. Rearranging the above inequality for energy and multiplying both the top and bottom of the fraction by c the speed of light we get,

$$\Delta E > \frac{\hbar c}{c\Delta t} \approx \frac{\hbar c}{r_S}$$

where r_S is the interaction distance of the strong force. Heisenberg's energy time uncertainty is valid for any "real particle", however, quantum mechanics allows us to violate this inequality by restating the above inequality in a contrapositive way so that the relation reads, for short time or length periods the energy must be less than or equal to some exchange energy E_{ex} so that,

$$E_{ex} \leq \frac{\hbar c}{r_S}$$

An estimation of the upper bound for the lowest energy exchange particle can be calculated using some empirical data. Calculating the binding between the proton and neutron, which minimizes the influence of the electromagnetic interaction, forming a deuteron. From experiment the radius of the deuteron is, $r_D = 1.95$ fm. We calculate the distance between the centers of each nucleon by subtracting the proton and neutron radii, $r_p = 0.8$ fm and $r_n = 0.3$ fm, from the diameter of the deuteron. Using $\hbar c = 197$ MeV·fm we get an exchange energy of,

$$E_{ex} \leq \frac{\hbar c}{r_S} \approx \frac{\hbar c}{2r_D - r_p - r_n} = 140.7 \text{ MeV}$$

So the energy of an exchange particle necessary to bind a proton and neutron together must not be greater than ≈ 140 MeV. This is similar to the result found by Yukawa and corresponds to the lightest meson $\pi^0 = 135$ MeV. We now see a similarity between QED and the strong force. In QED the exchange of a virtual photon mediates the electromagnetic interaction, this is analogous to result above where the exchange of a virtual pion mediates the strong interaction. However, this is not the whole story since it was later found that the pion is simply a consequence of a more fundamental theory of quarks, which are the building blocks of hadrons.

It is now well known that all fundamental interactions, save for gravity, are due to some exchange of virtual quanta. The advantage to using Coulomb excitation is that we can exclude these internal interactions dominated by the strong force thereby simplifying our calculations. We now consider an important excitation where a large number of constituent nucleons are excited into a quasi-stable state. These excitations are highly dependent on the number of nucleons, A, implying a dependence on the binding energy.

3.1 Giant Resonance

The large bulk nuclear response exhibited in nuclei with more than a few nucleons is known as a Giant Resonance (GR). The GR phenomenon has been shown to be a fundamental property of all nuclei [3,4,24] where the general features are; smooth transitions in the form, width, and centroid energy correlating to a change in the mass number A. The width is small compared to its excitation energy, and exhausts a large portion of the energy-weighted sum rule.

GR excitations are sensitive to several variable parameters available to the experimenter. The first, and probably most obvious, would be the isotopes used in the reaction (e.g. p+Pb, Pb+Pb, Ni+Au, ...). The energy of the collision and the characteristics of the beam are then adjusted and selection of the scattering angle reveals the cross sections of interest. The GR observed varies according to the excitation energies giving a cross section

$\sigma(E_\gamma)$, for excitation energy E_γ, which can be fit by a Lorentzian,

$$\sigma(E_\gamma) = \frac{\sigma_0 E_\gamma^2 \Gamma^2}{(E_\gamma^2 - E_C^2)^2 + E_\gamma^2 \Gamma^2} \tag{3.32}$$

for the Giant Dipole Resonance (GDR). The centroid energy, E_C, is the most probable energy of the resonance, e.g., ~ 24 MeV for ^{16}O and ~ 13 MeV for ^{208}Pb. The isotope excited into a resonance determines; the value of σ_0 which satisfies the sum rules, and the width Γ which varies from ~ 4 to 8 MeV. For different multipole excitations, (e.g., E1, E2, M1, M2, ...) the above parameters are adjusted accordingly.

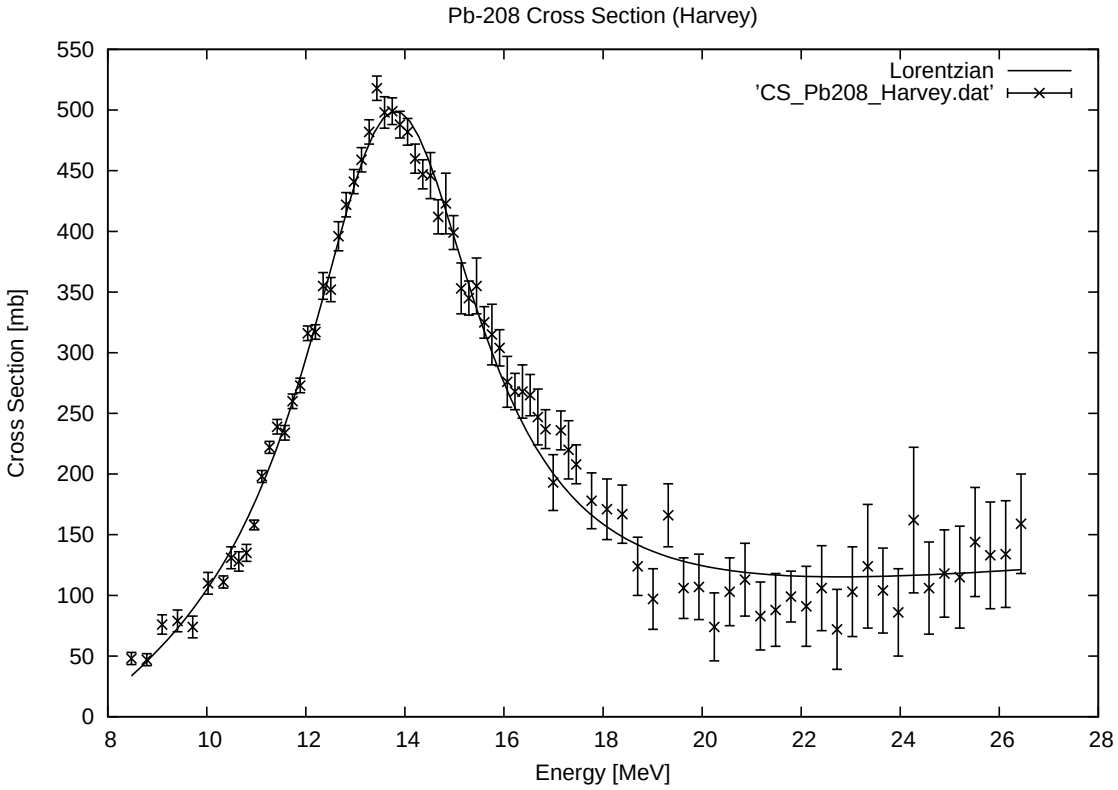

Figure 3.5. Example cross section for the GR in Lead-208.

In figure 3.5 a schematic for a typical photo-absorption cross section is given. At low energies the system exhibits discrete states which are characterized by surface effects due to

deformation, vibration, rotation, and a mixing of vibration and rotation. Around 8 MeV the discrete states give way to a continuum of states with the GDR, a dominant feature of the spectrum, appearing at around 8 MeV higher than where the continuum states begin.

These collective excitations involve an appreciable number of nucleons and are built up from individual excitations from the ground state of the nucleus.

3.1.1 Classical models

Over the years several collective models have been developed to describe the bulk response of nuclear matter. The progression of the theory from classical approximations to more sophisticated many-body models has been long running. A typical classical model for the GR phenomenon was first developed by Goldhaber and Teller [25] and later improved by Steinwedel and Jensen [26].

Three possible explanations for the features which define a GR are:

- A restoring force between the displaced protons and neutrons exists which is independent of the size of the nucleus. This possibility is discarded due to experimental evidence which clearly indicates a dependence on the number of nucleons A.

- A difference between the proton and neutron densities within the nucleus. In this situation the surface of the nucleus is not affected and the restoring force is proportional to the gradient of the difference in density. This picture describes the Steinwedel-Jensen model.

- Two spheres comprised of either protons or neutrons oscillate against one another. This is a pure dipole mode picture with the overall density kept constant. This is the picture taken in the Goldhaber-Teller model.

In the Goldhaber-Teller (GT) model a collection of protons, influenced by an electric field realized as an impinging photon, takes the nucleus to an excited state. The major feature of the GR phenomenon is of course the GDR and is described in the GT model as a

collection of protons moving against a collection of neutrons with their relative oscillations being opposite in phase to one another. This model allows for the collection of protons and neutrons to interpenetrate while preserving their individual incompressibility. The interpretation as two oscillating fluids will be important for our later look into the pygmy dipole resonance.

The other interpretation developed by the Steinwedel-Jensen (SJ) model preserves the total density of the nucleus by separating the proton and neutron densities such that,

$$\rho_A(\mathbf{r}, t) = \rho_P(\mathbf{r}, t) + \rho_N(\mathbf{r}, t)$$

the variation in density is then introduced by the addition and subtraction of a fractional density term $\delta\rho(\mathbf{r}, t)$ and requiring that the number of particles is conserved,

$$\int d^3r \ \delta\rho(\mathbf{r}, t) = 0$$

A shift in the distribution of positive charge is the central idea behind both pictures of the GDR developed by GT and SJ. Each model describes the phenomenon reasonably well with the SJ giving an A dependence as $A^{-1/3}$ which describes the experimental data better than GT's $A^{-1/6}$ dependence. Each of these models takes a classical approach to this dynamic quantum system. For a more complete picture one must include quantum mechanics.

Quantum mechanically describing the collective oscillations of many-particle systems is an interesting and challenging problem in nuclear physics. In the days before computer simulations, when quantum electrodynamics was first being developed, describing the dynamics of the wave functions for each individual nucleon inside of a nucleus was the stuff of dreams. Simplifications to the model and exploiting the symmetries and bulk properties of the system were necessary. Thus techniques such as mean field approximations where used to reduce the degrees of freedom to a solvable problem.

3.1.2 Microscopic Models

Although the classical models above describe the GDR reasonably well it is still necessary to extend this into a microscopic picture. Several effective theories exist which describe the GR on a microscopic level. Early attempts at calculations were developed based on the linear response theory [31]. Nowadays, an effort is being undertaken to describe nuclear collective motion with more elaborate models such as the time-dependent superfluid local density approximation [32, 33]. Similarly, theoretical studies of the pygmy resonances have been developed based on the improvements of the hydrodynamical model [34–36], and with microscopic theories such as the random phase approximation (RPA) and its variants [37–40].

Sum Rules

It is often useful to estimate the photoabsorption cross section over every transition from some initial state $|i\rangle \rightarrow |f\rangle$ to the possible final states. The estimate is found by the sum rule for the system and is given in the form,

$$\mathcal{S}_i^{(n)}[F] = \frac{1}{2}\sum_f (E_f - E_i)^n \left\{ \left| \langle f|F|i\rangle \right|^2 + \left| \langle i|F^\dagger|f\rangle \right|^2 \right\}$$

The sum rules give a tool for calculating the sum of integral cross sections for real photons over all possible final states.

3.2 Pygmy Dipole Resonance

Inherent to the majority of nuclei, excitation of the GR is a well investigated phenomenon. As the ratio of neutrons to protons increases the distribution of protons and neutrons begins to differ. Experiments which infer the radius of the nucleus typically involve the measurement of elastically scattered particles from the target.

The standard ways of measuring the radius of nuclei are easily understood through

classical scattering. To observe any reasonable detail of the nucleus the wavelength of the projectile must be smaller than the target. Suppose we wish to measure the radius of ^{208}Pb. According to the radius formula,

$$R = R_0 A^{1/3}$$

where $R_0 = 1.2 - 1.25$ fm, the radius of Lead 208 is $R_{Pb} \simeq 7$ fm, therefore the wavelength of the projectile must be $\lambda \leq 2R_{Pb} \simeq 14$ fm which corresponds to a projectile momentum of $p \geq 89$ MeV/c. High-energy electron experiments are able to achieve beam energies from 100 MeV to 1 GeV and are a good candidate for measuring the nuclear radius. Spectroscopic analysis of only the elastically scattered electrons gives a good average estimate to the charge radius of nuclei.

The electron projectiles are scattered by Coulomb interactions. This means that electron scattering tells us about the distribution of charge, i.e., protons, in the nucleus. Measurements of the distribution of all nuclear matter, which incorporates the protons and the neutrons, requires us to overcome the Coulomb barrier. Alpha particle scattering is one method where this is achieved. Using the classical scattering formula (2.16) developed by Rutherford form his famous alpha particle scattering experiments. Increasing the energy of the alpha projectiles the scattering cross section is well described by (2.16), however, at a certain energy the predictions of Rutherford's scattering formula are no longer accurate due to the effects of the nuclear force.

The results of these measurements show that the root mean square (rms) charge radius is almost the same as the rms nuclear radius differing by less than 1 fm. Since nuclei tend to have more protons than neutrons this implies that the protons distribute themselves across the nucleus leaving more neutrons to occupy the core.

When the number of neutrons become much larger than the number of protons the neutrons are then pushed out, due to their occupation pressure, beyond the rms charge radius creating a neutron rich layer. The difference between these two radii is called the neutron skin, $\Delta R_{Skin} = R_n - R_p$.

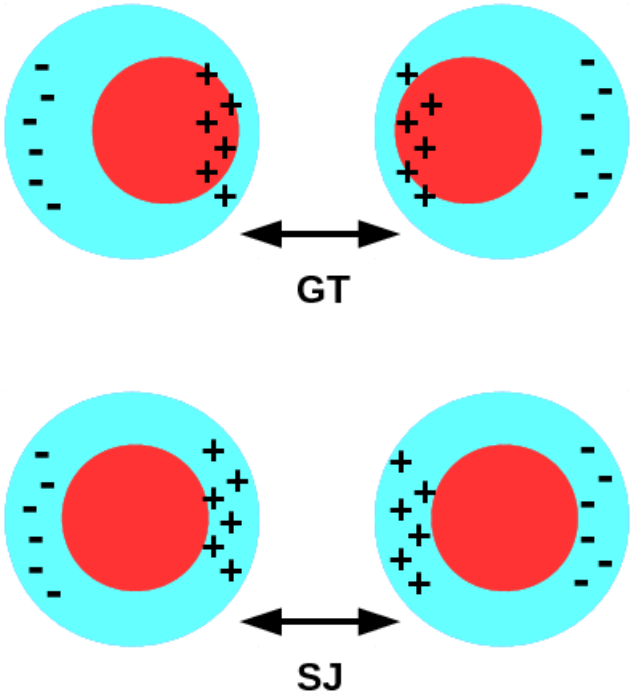

Figure 3.6. The dipole mode of the pygmy resonance in the Goldhaber-Teller (GT) and Steinwedel-Jensen (SJ) modes.

In reactions which involve neutron-rich nuclei at low excitation energies, close to the low energy tail of the GR, the excitation of the neutron skin against a symmetric nuclear core is observed. This phenomenon is known as the Pygmy Dipole Resonance (PDR) and can easily be visualized through the GT and SJ models as shown in figure 3.6.

Understanding the PDR is import since it can be used as a tool to constrain the neutron skin thickness of these neutron-rich nuclei. How the PDR is related to the neutron skin is through the fraction of the Energy Weighted Sum Rule (EWSR) exhausted by the PDR [27].

Measurements of the neutron skin have far reaching implications including areas of interest such as nuclear structure [28], neutron star structure [29], and heavy-ion collisions [30].

Chapter 4

PRESENTATION OF FINDINGS

(*Published in Physics Letters B, Volume* ***757****, 10 June 2016, Pages 553-557*)

As research on nuclear reactions with radioactive beams became the focus over the last few decades, it became apparent that modifications of the linear response theory predict a significant concentration in neutron-rich nuclei at low energies of the excitation strength [41,42]. It is important to note that the amount of energy of the nuclear response exhausted by the sum rule strongly depends on how the nuclear interaction, pairing, and other physical phenomena are incorporated in the theory [37–42]. As an example, the E1 strength function numerically calculated using the public code of Ref. [43], is given as

$$S(E) = \sum_{\nu} \left| \langle \nu || \mathcal{O}_L || 0 \rangle \right|^2 \delta(E - E_\nu) \tag{4.33}$$

where an RPA configuration space is defined in terms of delta-function states ν and the operator $\mathcal{O}_L$ is an electromagnetic operator. A smearing of 1 MeV of the fragmented strength function is introduced which produces a continuous distribution, shown in Fig. 4.7 for the E1 response in ^{68}Ni. We used the option $\mathcal{O}_L = j_L(qr)$ in Eq. (4.33), where we take $q = 0.1 fm^{-1}$ to be a representation of the momentum transfer. More details can be found in Ref. [43]. In this case, the strength function has dimensions of MeV^{-1} and in the long-wave approximation $qr \ll 1$ it is proportional to the usual response for electric multipole operators. The calculation is performed for several Skyrme interactions, as shown in the figure. The arrow shows the position of the expected pygmy dipole resonance. The results presented in the literature, e.g. [37–42] show a greater response in the PDR energy range due to interactions and adaptations in the model space. There is currently no clear prediction of the exact location of the pygmy strength. It could be in the range of $7 - 12$ MeV for medium mass nuclei such as Ni isotopes. The amount of the sum rule exhausted by the pygmy

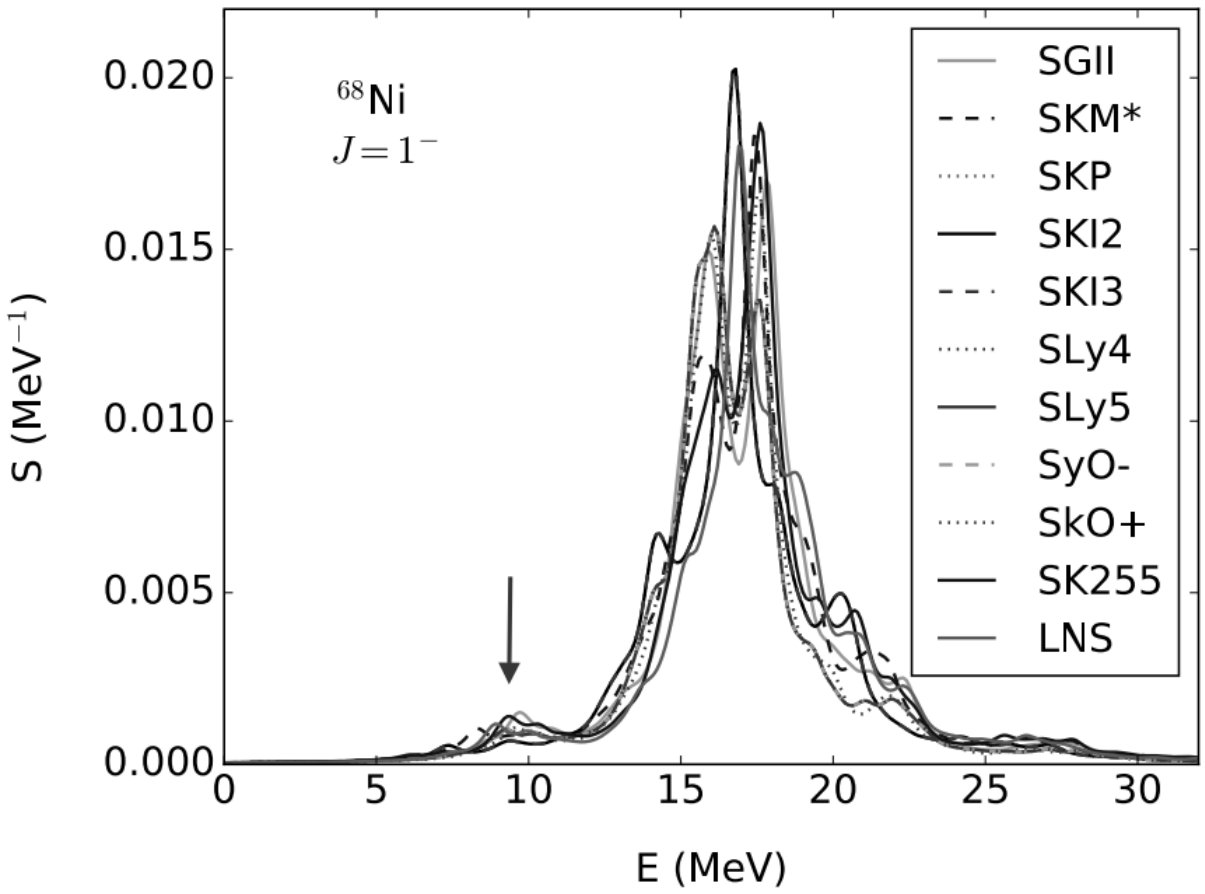

Figure 4.7. Strength function for the E1 RPA response in ^{68}Ni calculated with formalism described in Ref. [43]. The calculation is performed for several Skyrme interactions, shown in the figure inset. The arrow shows the location of the pygmy resonance. (For interpretation of the references to color in this figure legend, the reader is referred to the web version of this article.)

resonance is also relatively unknown, although some models based on nuclear clustering can reach up to 10% of the total strength [44].

Coulomb excitation of pygmy resonances is one of the effects overseen by the experimental analysis of these reactions. The large excitation probability in Coulomb excitation at small impact parameters leads to a strong coupling between the pygmy and giant resonances. A manifestation of this coupling is seen as dynamical effects such as the modification to transition probabilities and cross sections of the PDR. Previous observations of this coupling effect are seen in the excitation of double giant dipole resonances (DGDR) [1, 45, 46]. The experimental observation of the DGDR is a consequence of higher-order effects in relativis-

tic Coulomb excitation arising due to the large excitation probabilities of giant resonances in heavy ion collisions at small impact parameters. The dynamical coupling between the usual giant resonances and the DGDR is very strong, as shown, e.g., in Ref. [22]. In the present work this dynamical coupling effect on the excitation of the PDR is assessed using the relativistic coupled channels (RCC) equations introduced in Ref. [47].

The S-matrix for state α given as, $S_\alpha(z,b)$, is obtained from the RCC equations [47]

$$i\nu\frac{\partial S_\alpha(z,b)}{\partial z} = \sum_{\alpha'}\langle\alpha|\mathcal{M}_{EL}|\alpha'\rangle S_{\alpha'}(z,b)e^{-i(E'_\alpha - E_\alpha)z/\hbar\nu}, \tag{4.34}$$

where ν is the projectile velocity and $\mathcal{M}_{EL}$ is the electromagnetic operator for transitions by the electric dipole (E1) and quadrupole (E2) modes connecting states α and α'. The states must satisfy the intrinsic angular momenta and parity selection rules. The ground state is denoted as $|0\rangle = |E_0 J_0 M_0\rangle$ and the excited states by $|\alpha\rangle = |E_\alpha J_\alpha M_\alpha\rangle$ where EJM are the intrinsic energy and angular momentum quantum numbers. The electromagnetic operators, in the long-wavelength approximation, are given by [47]

$$\mathcal{M}_{E1m} = \sqrt{\frac{2\pi}{3}}\xi Y_{1m}(\hat{\xi})\frac{\gamma Z_T e^2}{(b^2+\gamma^2 z^2)^{3/2}}\begin{cases}\mp\, b & (\text{if } m=\pm 1)\\ \sqrt{2}\,z & (\text{if } m=0)\end{cases} \tag{4.35}$$

where ξ is the intrinsic coordinate of the excited nucleus and Ze is the charge of the nucleus creating the interacting electromagnetic field (in our case, the target). The electromagnetic operator for E2 transitions is [47]

$$\mathcal{M}_{E2\mu} = \sqrt{\frac{3\pi}{10}}\xi^2 Y_{2m}(\hat{\xi})\frac{\gamma Z_T e^2}{(b^2+\gamma^2 z^2)^{5/2}}\begin{cases} b^2 & (\text{if } \mu=\pm 2)\\ \mp 2\gamma^2 bz & (\text{if } \mu=\pm 1)\\ \sqrt{2/3}(2\gamma^2 z^2 - b^2)z & (\text{if } m=0)\end{cases} \tag{4.36}$$

We note that the electromagnetic operator is expressed as $\mathcal{M}_{ELm} = f_{ELm}(\mathbf{r})\mathcal{O}_{ELm}$, where

$\mathcal{O}_{ELm} = \xi_L Y_{Lm}(\hat{\xi})$ is the usual electric operator, and $f_{ELm}(\mathbf{r})$ is a function of the projectile-target relative position $\mathbf{r} = (\mathbf{b}, z)$.

Solutions to the coupled equations (4.34) are found by using $S_\alpha(z \to -\infty) = \delta_{\alpha 0}$. For collisions at high energies and very forward angles, the cross sections for the transition $|0\rangle \to |\alpha\rangle$ are given by

$$\frac{d\sigma_\alpha}{dE} = 2\pi w_\alpha(E) \int db\ b\ \exp[-2\chi(b)] \left| S_\alpha(z \to \infty, b) \right|^2 , \tag{4.37}$$

where $w_\alpha(E)$ is the density of final states, b is the impact parameter in the collision, and $\chi(b)$ is the eikonal absorption phase given by

$$\chi(b) = \frac{\sigma_{NN}}{4\pi} \int dq\ q \rho_1(q) \rho_2(q) J_0(qb) \tag{4.38}$$

where σ_{NN} is the total nucleon–nucleon cross section, obtained from experiment, with medium corrections added according to Refs. [48, 49]. The Fourier transform of the ground state densities of the nuclei, $\rho_i(q)$, is obtained from fitting to electron scattering experiments [50] for ^{197}Au and using Hartree–Fock–Bogoliubov calculations with the SLy4 interaction for ^{68}Ni. A reduction of the Coulomb excitation mechanism at small impact parameters, first introduced in Ref. [51], is used to calculate reaction cross sections relevant to excitations of the GDR and DGDR. To remain within the contexts of current experimental results we neglect effects of nuclear excitations, and possible interferences which were subtracted in experiments [52–54].

To facilitate our discussions we consider the excitation of ^{68}Ni on ^{197}Au and ^{208}Pb targets at 600 and 503 MeV/nucleon, respectively. These reactions have been experimentally investigated in Refs. [52,53]. In the first experiment the pygmy dipole resonance was observed at $E_{PDR} \simeq 11$ MeV with a width of $\Gamma_{PDR} \simeq 1$ MeV, for ^{68}Ni and exhausted about 5% of the Thomas–Reiche–Kuhn (TRK) energy-weighted sum rule. The excitation was identified through the analysis of its decay product, gamma emission. The second experiment found

the PDR centroid energy to be at 9.55 MeV, width a of 0.5 MeV and exhausting 2.8% of the TRK sum rule. The PDR was identified by measuring the neutron decay channel of the PDR. This studies focus will be on the effects of coupling between the different modes of giant resonances with the PDR. Therefore, we will not take into consideration the decay channels but restrict our analysis to the calculation of the excitation function $d\sigma/dE$.

A model is needed for including the bound and continuum discretized wavefunctions in the matrix elements of $\langle\alpha|\mathcal{M}_{EL}|\alpha'\rangle$ in Eq. (4.34). To calculate the response functions, $dB_{EL}/dE = \sum_{spins} w_{\alpha'} \left|\langle\alpha||\mathcal{O}_{EL}|\,|\alpha'\rangle\right|^2$, it is appropriate to use these wavefunctions, with obvious consideration for summing over angular momentum coefficients. To simplify calculations we assumed Lorentzian forms for the response functions dB_{EL}/dE and assign an appropriate fraction of the sum-rule based on current experimental values. We then discretized the functions into energy bins to obtain the reduced matrix elements $\left|\langle\alpha||\mathcal{M}_{EL}|\,|\alpha'\rangle\right|^2 \propto \Delta E_\chi (dB_{EL}/dE)\big|_{E=E_\chi}$, where $E_\chi = E_{\alpha'} - E_\alpha$. To keep everything in terms of real numbers a phase convention is found for the reduced matrix elements. These are then used, with proper care taken for the corresponding angular momentum coefficients, in determining the matrix elements $\langle\alpha|\mathcal{M}_{EL}|\alpha'\rangle$ in Eq. (4.34) (see, e.g., Ref. [46]).

The Lorentzian functions are described by Eq. (3.32) with their respective centroid energies E_{PDR} for pygmy dipole resonances and E_{GDR} (E_{GQR}) for the isovector (isoscalar) giant dipole (quadrupole) resonances. Their respective widths are denoted by Γ_{PDR}, Γ_{GDR} and Γ_{GQR}. The discretized strength function is subdivided into 35 energy bins centered around each resonance. The PDR centroid energy $E_{PDR} = 11$ MeV is chosen, consistent with Refs. [52,53]. However, a full width at half maximum of 2 MeV was chosen, which is more in line with theoretical calculations [35–42] than with the experimental data [52,53]. Our choice to use the theoretical width was in essence made to better determine higher-order effects on the modified tails of the PDR without changing the other aspects of the PDR appreciably. For the major mode of the GR the (isovector) 1^- giant dipole resonance (GDR) was given a centroid energy and width of $E_{GDR} = 17.2$ MeV and $\Gamma_{GDR} = 4.5$ MeV, respectively. For the

(isoscalar) 2^+ giant quadrupole resonance (GQR) we take $E_{GQR} = 15.2$ MeV and $\Gamma_{GQR} = 4.5$ MeV. The centroid and width for the GQR are approximations based on the systematics of GQR excitation in nickel isotopes [55] and are not experimental values. Looking at the total number of channels involved in our calculation we have, $35 \times 3 + 35 \times 5 + 35 \times 5 + 1 = 456$ which includes all magnetic substates plus an additional channel for the 0^+ ground state. For practical purposes, to reduce computational intensity, considering only the major dynamical effects arising from the coupling of the PDR with the GQR via the dominant E1 interaction at relativistic energies. A reduction by a factor of 2 is possible by implementing a coarser binning of the PDR and GQR states introducing only a loss of accuracy at the level of 10%. Calculations using all the channels above will converge to within 1%.

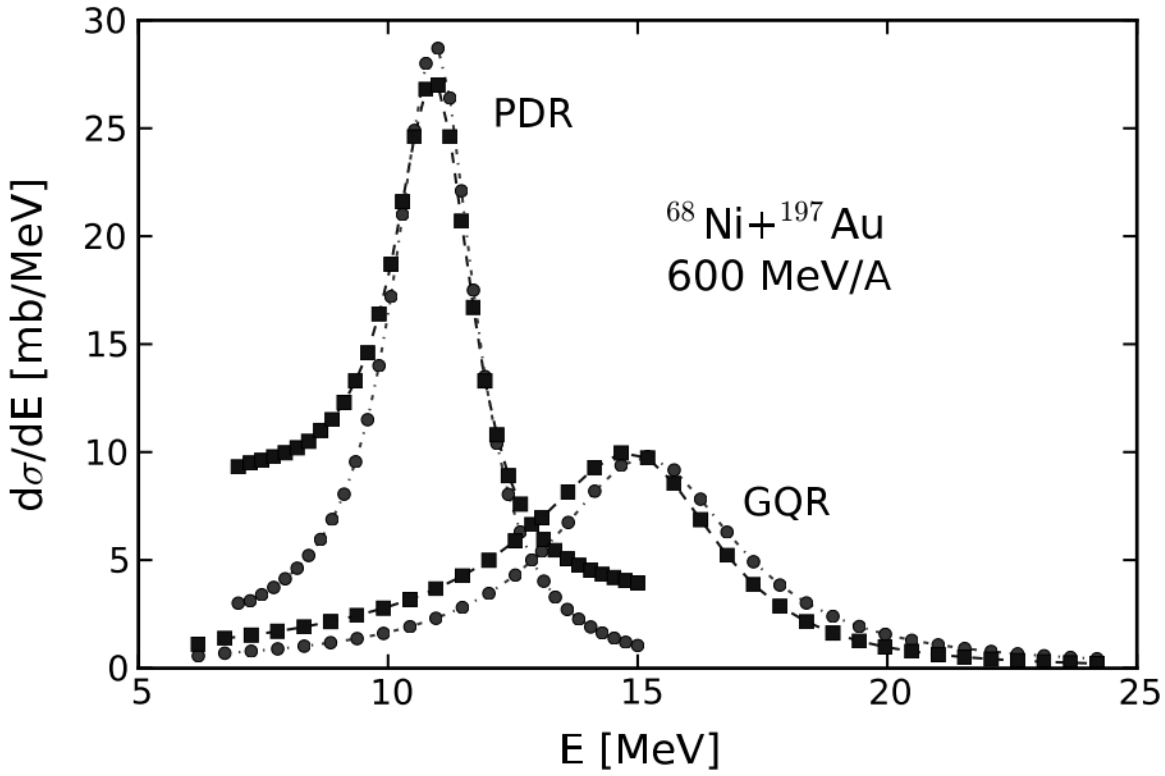

Figure 4.8. Coulomb excitation cross section as a function of the excitation energy of 600 MeV/nucleon ^{68}Ni projectiles incident on ^{197}Au targets. The filled circles represent the calculations using first-order perturbation theory, while the filled squares are the results of coupled-channel calculations.

In Fig. 4.8 we show, for 600 MeV/nucleon ^{68}Ni projectiles incident on ^{197}Au targets,

the first-order Coulomb excitation cross sections as a function of the excitation energy for the PDR and GQR separately. Calculations using first-order perturbation theory are denoted by filled circles, while the filled squares represent the coupled-channel calculations. The first-order Coulomb excitation cross sections, as shown in Ref. [**?**], can be obtained by means of the relation

$$\frac{d\sigma}{dE} = \sum_{\pi L} \frac{N_{\pi L}(E)}{E} \sigma_{\pi L}^{(\gamma)}(E) \tag{4.39}$$

where $N_{\pi L}$ are the virtual photon numbers of multipole πL and $\sigma_{\pi L}^{(\gamma)}$ are the real photon cross sections with multipolarity πL. The virtual photon numbers include the same absorption coefficient as in Eq. (4.37) [51]. Summing over the relevant multipoles, here E1 and E2 stand for 1^- and 2^+ excitations, respectively. The figure shows that the coupling between these states has a visible impact on the energy dependence of the cross sections. According to the Brink–Axel hypothesis, the excitation of a giant resonance on top of any other state in a nucleus is possible [56, 57]. Therefore, the couplings are a manifestation of $(\mathrm{PDR}\otimes\mathrm{GQR})_{1^-}$, $(\mathrm{PDR}\otimes\mathrm{PDR})_{2^+}$, $(\mathrm{PDR}\otimes\mathrm{GDR})_{2^+}$ and $(\mathrm{GDR}\otimes\mathrm{GQR})_{1^-}$ states which we investigate, as they build up components of the PDR, GDR and GQR. Our findings suggest the importance for the reliable extraction of the experimental strength of the PDR relative to the GDR.

The dynamical calculations show that both the strength and width of the PDR are modified appreciably due to the coupling to the GQR. Fig. 4.8 shows separately that the population of PDR and GQR states are modified. The 1^- states in the GDR region are affected very weakly and so are left out of the figure. In the high energy region the GDR excitation dominates by a factor of 2–3 times that of the 2^+ states. The important modifications in the excitation spectrum appear from the couplings PDR$\leftrightarrow$GQR$\leftrightarrow$PDR by E1 fields, while couplings from PDR$\leftrightarrow$GDR$\leftrightarrow$PDR by E2 fields contribute very little to the 1^- states in the PDR energy region. In Fig. 4.8 we notice that the tails of the PDR, and to a lesser extent those of the GQR, are appreciably modified. A small shift to the peaks is also seen, although barely visible for the PDR, it is evident for the GQR. It is important to also keep in mind that the strength and shape of the PDR will also be modified by the low energy

tail of the GDR. For our case considered here, a GDR strength on the order of 3.8% lies within the region of the PDR meaning that the PDR shape will only slightly be influenced by this low energy tail. However, these effects have been considered in the experimental analyses [52, 53]. In this work we are interested in the higher-order effects which have been so far ignored.

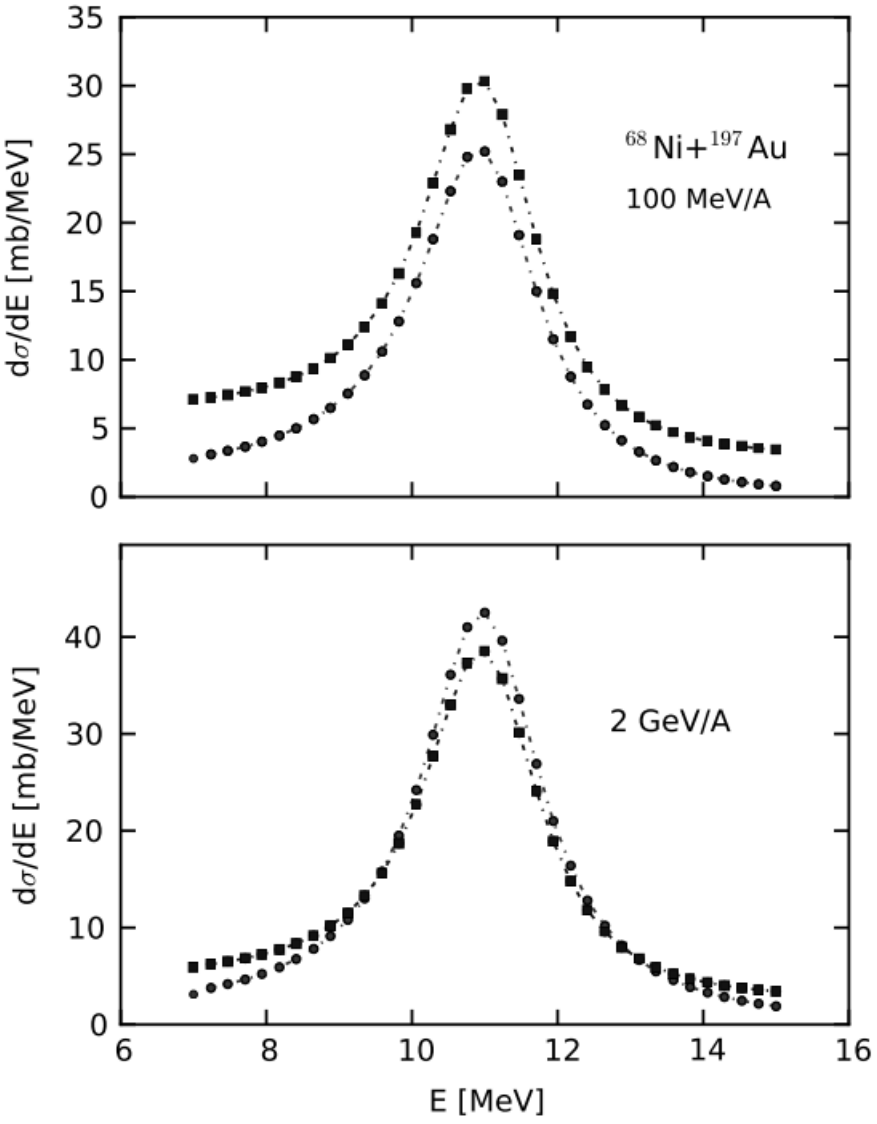

Figure 4.9. Coulomb excitation cross section as a function of the excitation energy of ^{68}Ni projectiles incident on ^{197}Au targets at two laboratory energies. The filled circles represent the calculations using first-order perturbation theory, while the filled squares are the results of coupled-channel calculations.

In Fig. 4.9 the energy region of the pygmy resonance has been singled out and we

plot the results of our calculations for two different bombarding energies: 100 MeV/nucleon and 2 GeV/nucleon, using the same notation as in Fig. 4.8. The coupling effects change dramatically. For the lower energy interaction the influence of the giant resonances increases appreciably for the response in the energy region of the PDR, while at the higher energy collision this effect is much smaller and shows a slight tendency th decrease the PDR excitation cross section. This is expected since for energies around 100 MeV/nucleon the E2 field is dominant, with an increase to the excitation of the GQR and consequently a strong feedback to the PDR from subsequent E1 transitions.

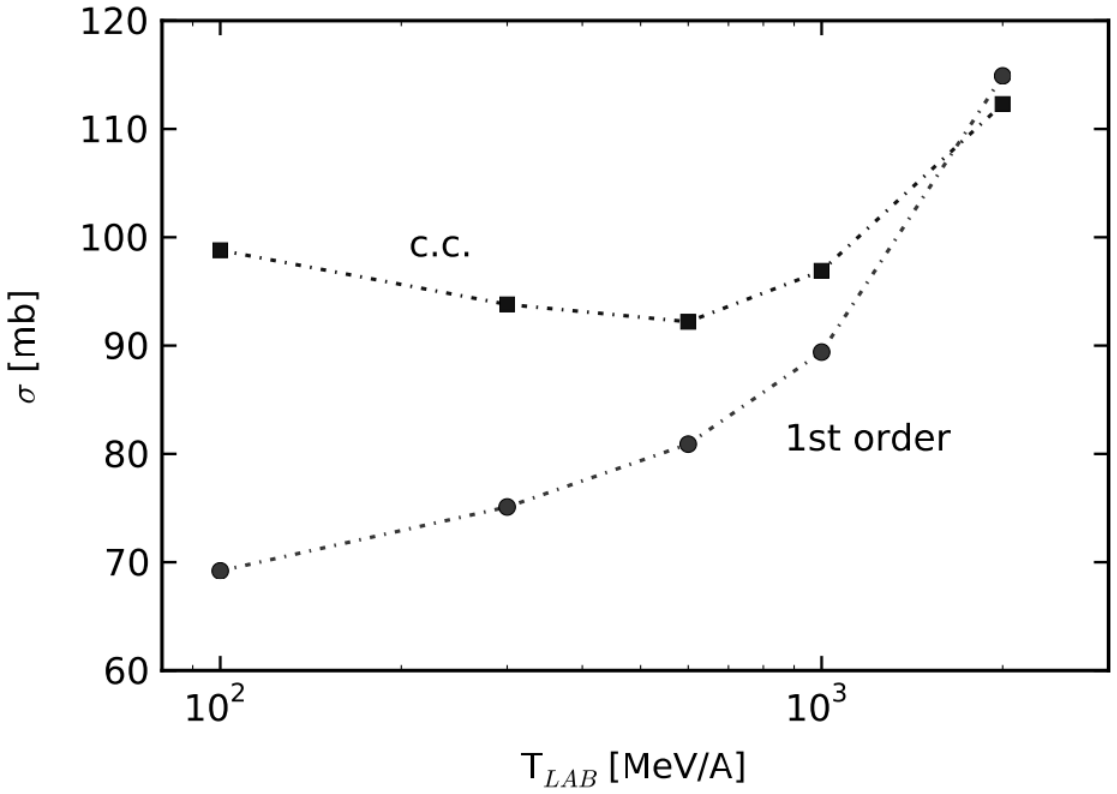

Figure 4.10. Coulomb excitation cross sections of the PDR as a function of the bombarding energy of ^{68}Ni projectiles incident on ^{197}Au targets. The filled circles represent the calculations using first-order perturbation theory, while the filled squares are the results of coupled-channel calculations.

The Coulomb excitation cross sections of the PDR as a function of the bombarding energy of ^{68}Ni projectiles incident on ^{197}Au targets is given in Fig. 4.10. Calculations using first-order perturbation theory are represented by the filled circles, while the filled squares

are the results of our coupled-channel calculations. Its apparent that at lower energies the deviation is more pronounced. At 600 MeV/nucleon the cross section for excitation of the PDR changes from 80.9 mb obtained with the virtual photon method to 92.2 mb with the coupled-channels calculation. A reflection of this effect in the extracted PDR strength from the experimental data amounts to an appreciable change of 14%. This reduction is approximately the same amount of the strength needed to reproduce the experimental data.

Calculations have also performed for ^{68}Ni + ^{208}Pb at 503 MeV/nucleon, corresponding to the experiment of Ref. [53]. To first-order, the Coulomb excitation cross section for the PDR in ^{68}Ni is found to be 58.3 mb, with the inclusion of the effects of coupling to the giant resonances, the cross section increases to 71.2 mb, i.e., an important 18.1% correction. The dipole polarizability is defined as

$$\alpha_D = \frac{\hbar c}{2\pi^2} \int dE \frac{\sigma(E)}{E^2} \tag{4.40}$$

where $\sigma(E)$ is the photo-absorption cross section. From Ref. [53] the extracted experimental value of α_D is 3.40 fm^3 while in order to reproduce the experimental cross section with our dynamical calculations we have α_D = 3.16 fm^3, a small but non-negligible correction. Assuming a linear relationship between the dipole polarizability and the neutron skin [58], a reduction to the neutron skin from 0.17 fm, as reported in Ref. [53], to 0.16 fm is expected. A correction such as this lies within the experimental uncertainty of 7% for α_D and 0.02 fm for the neutron skin [53]. However, consideration of the coupling effects should be taken into account in the future as more precise data becomes available, in particular, if the measurement is performed at lower bombarding energies.

Chapter 5

CONCLUSIONS

We conclude that probabilities of giant resonances due to the large Coulomb excitation in heavy ion collisions at energies around and above 100 MeV/nucleon, the excitation of the PDR is also modified due to the coupling between the 1^- and 2^+ states. Our calculations, utilizing a Lorentz-like distribution for simplicity of the electromagnetic response and sum-rules, are carried out without a detailed nuclear structure model. Future investigations carried out for nearly "ab-initio" calculations based on a microscopic theory, coupled with a proper reaction mechanism, might be possible. A known alternative using individual states calculated by RPA or other microscopic models together with higher order perturbation theory, have already used in previous studies of multiphonon resonances [59]. Finally, the use of an advanced mean-field time-dependent method such as that developed in Ref. [33] is also available. Deriving rather accurate dipole strength distributions from the electromagnetic excitation of the PDR is mainly of relevance to the extraction of the dipole polarizability [53], which is an important observable for constraining the symmetry energy, and is thus also important for better understanding the properties of neutron-stars. A particularly important aspect for the polarizability is the low-energy response due to the inverse weighting with energy. This opens exciting possibilities for studies of the pygmy resonance in nuclei and its use as a tool for applications in nuclear astrophysics.

References

[1] C.A. Bertulani and G. Baur, Phys. Rep. **163**, 299 (1988).

[2] K. Goeke and J. Speth, Annu. Rev. Nucl. Part. Sci. **32**, 65 (1982).

[3] Carlos A. Bertulani, *Nuclear Physics in a Nutshell*, (Princeton University Press, NJ, 2007).

[4] W. Greiner and J. A. Maruhn, *Nuclear Models*, (Springer-Verlag, Berlin Heidelberg, 1996).

[5] T. Aumann, Phys. Eur. J. A **26**, 441 (2005).

[6] J. Piekarewicz, Phys. Rev. C **73**, 044325 (2006), nucl-th/0602036.

[7] T. Nomura, S. Kubono, *Soft Giant Resonance*, Experimental proposal to the Japanese Hadron project (now J-PARC), June 1987

[8] K. Ikeda, INS Report **JHP-7**, 1988 (in Japanese);
K. Ikeda, Nucl. Phys. A **538**, 355c (1992).

[9] C.A. Bertulani, M.S. Hussein, Phys. Rev. Lett. **64**, 1099 (1990).

[10] Kenneth S. Krane, *Introductory Nuclear Physics*, 3rd ed. (Wiley, 1988).

[11] John David Jackson, *Classical Electrodynamics*, 3rd ed. (Wiley, 1999).

[12] G. Baur and C.A. Bertulani, Phys. Lett. B **174**, 23 (1986).

[13] James Clerk Maxwell, *A Treatise on Electricity and Magnetism, Vol. 1*, 3rd ed. (Dover Publications, 1954).

[14] James Clerk Maxwell, *A Treatise on Electricity and Magnetism, Vol. 2 (Classic Reprint)*, (Forgotten Books, 2016).

[15] Michael E. Peskin and Daniel V. Schroeder, *An Introduction to Quantum Field Theory*, (Westview press, 1995).

[16] Richard P. Feynman and Albert R. Hibbs, editors Daniel F. Styer, *Quantum Mechanics and Path Integrals*, emended ed. (Dover Publications, Mineola, NY, 2005).

[17] Goldstein, Safko, and Poole, *Classical Mechanics*, 3rd ed. (Pearson Education, 2014).

[18] Francis Eugene Low, *Classical field theory: electromagnetism and gravitation*, (John Wiley & Sons, 1997).

[19] E. Fermi, Z. Physik, **29**, 315 (1924).

[20] E. Fermi, Nuovo Cimento **2**, 143 (1925).

[21] C.F. Weizsacker, Z. Physik, 612 (1934);
E.J. Williams, Phys. Rev. **45**, 729 (1934).

[22] C.A. Bertulani, L.F. Canto, M.S. Hussein and A.F.R. de Toledo Piza, Phys. Rev. C **53**, 334 (1996).

[23] H. Yukawa, Proc. Phys. Math. Soc. Jap. **17**, 48 (1935).

[24] Kurt A. Snover, Ann. Rev. Nucl. Part. Sci. **36**, 545 (1986).

[25] M. Goldhaber and E. Teller, Phys. Rev. **74**, 1046 (1948).

[26] H. Steinwedel and H. Jensen, Z. Naturforschung 5A, 413 (1950).

[27] N. Tsoneva and H. Lenske, Phys. Rev. C **77**, 024321 (2008).

[28] B. A. Brown, Phys. Rev. Lett. **85**, 5296 (2000).

[29] C. J. Horowitz and J. Piekarewicz, Phys. Rev. Lett. **86**, 5647 (2001), astro-ph/0010227.

[30] M. B. Tsang et al., Phys. Rev. Lett. **92**, 062701 (2004).

[31] M. Baranger, Phys. Rev. **120**, 957 (1960).

[32] A. Bulgac, Annu. Rev. Nucl. Part. Sci. **63**, 97 (2013).

[33] I. Stetcu, et al., Phys. Rev. Lett. **114**, 012701(2015).

[34] Y. Suzuki, K. Ikeda, H. Sato, Prog. Theor. Phys. **83**, 180 (1990).

[35] D. Vretenar, et al., Nucl. Phys. A **692**, 496 (2001).

[36] C.A. Bertulani, Phys. Rev. C **75**, 024606 (2007);
C.A. Bertulani, Nucl. Phys. A **788**, 366 (2007).

[37] N. Paar, D. Vretenar, E. Khan, G. Colò, Rep. Prog. Phys. **70**, 691 (2007).

[38] S. Krewald, J. Speth, Int. J. Mod. Phys. E **18**, 1425 (2009).

[39] V.Yu. Ponomarev, J. Phys. Conf. Ser. **533**, 012028 (2014).

[40] P. Papakonstantinou, H. Hergert, V. Yu Ponomarev, R. Roth, Phys. Rev. C **89**, 034306 (2014).

[41] G. Bertsch, J. Foxwell, Phys. Rev. C **41**, 1300 (1990);
G. Bertsch, J. Foxwell, Phys. Rev. C **42**, 1159 (1990) (Erratum).

[42] N. Teruya, C.A. Bertulani, S. Krewald, H. Dias, M.S. Hussein, Phys. Rev. C **43**, 2049 (1991).

[43] G. Colò, L. Cao, N.V. Giai, L. Capelli, Comput. Phys. Commun. **184** 142 (2013).

[44] Y. Alhassid, M. Gai, G.F. Bertsch, Phys. Rev. Lett. **49**, 1482 (1982).

[45] T. Aumann, P.F. Bortignon, H. Emling, Annu. Rev. Nucl. Part. Sci. **48**, 351 (1998).

[46] C.A. Bertulani, V. Ponomarev, Phys. Rep. **321** (1999).

[47] C.A. Bertulani, Phys. Rev. Lett. **94**, 072701 (2005).

[48] C.A. Bertulani, C. De Conti, Phys. Rev. C **81**, 064603 (2010).

[49] Mesut Karakoc, A. Banu, C.A. Bertulani, L. Trache, Phys. Rev. C **87**, 024607 (2013).

[50] H. de Vries, C.W. de Jager, C. de Vries, At. Data Nucl. Data Tables 36, 495–536 (1987).

[51] T. Aumann, C.A. Bertulani, K. Suemmerer, Phys. Rev. C **51**, 416 (1995).

[52] O. Wieland, et al., Phys. Rev. Lett. **102**, 092502 (2009).

[53] D.M. Rossi, et al., Phys. Rev. Lett. **111**, 242503 (2013).

[54] D. Savran, T. Aumannnd, A. Zilges, Prog. Part. Nucl. Phys. **70**, 210 (2013).

[55] D.H. Youngblood, Y.-W. Lui, U. Garg, R.J. Peterson, Phys. Rev. C **45**, 2172 (1992).

[56] D.M. Brink, PhD thesis, Oxford University, (1955).

[57] P. Axel, Phys. Rev. **126**, 671 (1962).

[58] J. Piekarewicz, Phys. Rev. C **83**, 034319 (2011).

[59] V.Yu. Ponomarev, C.A. Bertulani, Phys. Rev. C **57**, 3476 (1998).

Vita

Since graduating in 2008 from Hendrickson High School, Nathan S. Brady spent the first two years exploring different career interests before discovering an obsession for physics. Nathan enrolled at The University of Nebraska at Kearney in 2010 where he pursued degrees in both physics and mathematics. There he was awarded several grants and awards including a NASA funded summer internship at the City College of New York. After graduating in 2014 Nathan enrolled at Texas A&M - Commerce to pursue a Master of Science in Physics. While attending he received several awards, including Outstanding Graduate Student and a summer Graduate Assistant Research. Nathan was also selected from a pool of candidates from around the world to participate in the TALENT workshop over the summer in Caun, France. In the Fall of 2016 Nathan was awarded the Master of Science degree and admitted into the PhD program at Texas A&M University - College Station.

Permanent address:

Nathan S. Brady

Department of Physics and Astronomy

Texas A&M University-Commerce

P.O. Box 3011

Email: bradynsb@gmail.com